nature neuroscience

A pathway from midcingulate cortex to posterior insula gates nociceptive hypersensitivity

Linette Liqi Tan[1], Patric Pelzer[2,7], Céline Heinl[1], Wannan Tang[3,7], Vijayan Gangadharan[1], Herta Flor[4,5], Rolf Sprengel[3,6], Thomas Kuner[2,5] & Rohini Kuner[1,5]

The identity of cortical circuits mediating nociception and pain is largely unclear. The cingulate cortex is consistently activated during pain, but the functional specificity of cingulate divisions, the roles at distinct temporal phases of central plasticity and the underlying circuitry are unknown. Here we show in mice that the midcingulate division of the cingulate cortex (MCC) does not mediate acute pain sensation and pain affect, but gates sensory hypersensitivity by acting in a wide cortical and subcortical network. Within this complex network, we identified an afferent MCC–posterior insula pathway that can induce and maintain nociceptive hypersensitivity in the absence of conditioned peripheral noxious drive. This facilitation of nociception is brought about by recruitment of descending serotonergic facilitatory projections to the spinal cord. These results have implications for our understanding of neuronal mechanisms facilitating the transition from acute to long-lasting pain.

© 2017 Nature America, Inc., part of Springer Nature. All rights reserved.

Imaging studies in humans and rodents have revealed the cingulate cortex to be consistently activated during pain perception[1–4]. *Ex vivo* electrophysiological recordings in rodent models of pain have demonstrated synaptic potentiation in the anterior cingulate cortex (ACC), suggesting the ACC is involved in pain memories[5]. However, the distinct cingulate subdivisions that can be delineated on the basis of cytoarchitecture, neurochemistry and connectivity, as well as differential activity patterns, have not been considered in most functional studies[2,6]. These include the rostral ACC (rACC), also referred to as the pregenual ACC, which is distinct from the subdivisions of MCC and the posterior cingulate cortex in the dorsal and caudal ACC, respectively[7]. How this anatomical diversity is translated into functional differences has not been considered in pain and may underlie the diverse putative functions described for the cingulate cortex in pain modulation[8–16].

Notably, the contributions of the MCC in pain have not been specifically interrogated, despite its consistent and marked activation in human subjects and patients demonstrating clinical deviations from normal pain sensitivity[2,17,18]. Moreover, mechanistic insights obtained by elucidating circuits and the identity of target regions in brain networks are entirely lacking.

Here we address the specific contributions of the MCC to nociception, acute pain and subacute plasticity of nociceptive processing using optogenetic manipulations, circuit mapping and functional interrogation in awake mice. Our results identify a pathway from the MCC to the posterior insula that gates adaptive sensory responses and their acute plasticity in pain without influencing pain affect or fear.

RESULTS

To investigate the role of the MCC during the development of acute pain and nociceptive plasticity in mice, we employed optogenetic tools to broadly manipulate the activity of excitatory input and output neurons across all layers of the MCC, targeting a well-defined area that is anatomically distinct from the rACC (**Fig. 1a** and **Supplementary Fig. 1**)[7]. We used the proton pump Archaerhodopsin (from *Halorubrum* strain TP009; ArchT) for silencing and the cationic channel Channelrhodopsin 2 (ChR2) for stimulating MCC neurons[19] via *Camk2a* promoter–driven expression using recombinant adeno-associated vectors (rAAVs) (rAAV-CaMKII-ArchT-Venus, **Fig. 1a**), reaching a transduction efficiency of about 80% of excitatory neurons. Efficacy of manipulating neuronal activity was ascertained via patch-clamp whole-call recordings from layer 2/3 pyramidal neurons in MCC slices derived from these mice, as well as *in vivo* tetrode recordings in awake, freely moving mice (**Fig. 1b–e** and **Supplementary Fig. 2**). Lack of toxicity on the part of the virus injection and photomanipulation was confirmed post-mortem by TUNEL staining, cell counts and electrophysiological analyses (**Supplementary Figs. 2** and **3**).

Injection of the strong algogen capsaicin into the hindpaw activated neurons in all layers of the MCC, as visualized by a robust increase in expression of the activity-induced protein c-Fos

[1]Institute of Pharmacology, Heidelberg University, Heidelberg, Germany. [2]Department of Functional Neuroanatomy, Institute for Anatomy and Cell Biology, Heidelberg University, Heidelberg, Germany. [3]Max Planck Institute for Medical Research, Department of Molecular Neurobiology, Heidelberg, Germany. [4]Department of Cognitive and Clinical Neuroscience, Central Institute of Mental Health, Medical Faculty Mannheim, University of Heidelberg, Mannheim, Germany. [5]CellNetworks Cluster of Excellence, Heidelberg University, Heidelberg, Germany. [6]Max Planck Research Group at the Institute for Anatomy and Cell Biology, Heidelberg University, Heidelberg, Germany. [7]Present addresses: Letten Centre and GliaLab, Department of Physiology, Institute of Basic Medical Sciences, University of Oslo, Oslo, Norway (W.T.) and Cologne Excellence Cluster on Cellular Stress Responses in Aging-Associated Diseases (CECAD), University of Cologne, Cologne, Germany (P.P.). Correspondence should be addressed to R.K. (rohini.kuner@pharma.uni-heidelberg.de).

Received 10 June 2016; accepted 15 August 2017; published online 18 September 2017; doi:10.1038/nn.4645

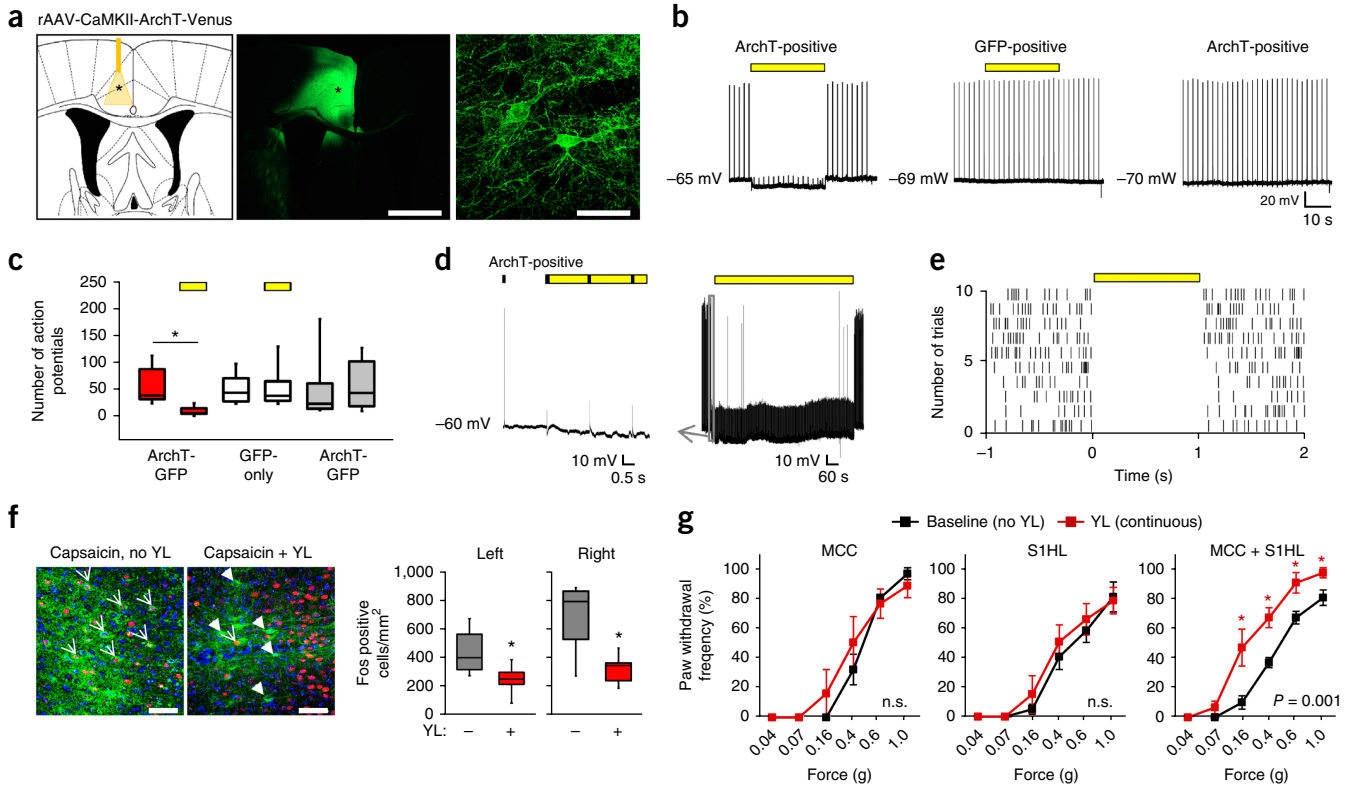

Figure 1 Optogenetic silencing of pain-related neuronal activity in MCC or/and S1HL, and its impact on nociception. (**a**) Left: viral expression of Venus-tagged ArchT and area of illumination with yellow light (YL) from an optic fiber tip (*) implanted in the MCC. Middle and right: examples of ArchT-expressing pyramidal neurons (scale bars, 1 mm and 50 µm, respectively). (**b**,**c**) Examples (**b**) and quantification (**c**) from *ex vivo* electrophysiological whole-cell recordings performed consecutively in the absence or presence of YL (yellow bars) in MCC slices in pyramidal neurons expressing ArchT-GFP (red bars; $n = 31$ cells, 8 mice; $U = 2.00$, $P < 0.001$), GFP only (white bars; $n = 13$ cells, 6 mice; $U = 92$, $P = 0.8$), or in ArchT-GFP cells (gray bars, showing consecutive recordings in the absence of YL; $n = 13$ cells, 6 mice; $P = 0.48$) during current injections at 0.5 Hz from 14 repeated 30-s trials. (**d**) Example traces from an ArchT-positive cell during 15-min current injections (black bars) and YL exposure. Left panel shows a magnification of the gray box on the right. (**e**) Raster plot of a spontaneously active MCC neuron inhibited by YL in electrophysiological recordings *in vivo* in an awake mouse expressing ArchT. (**f**) Examples (left) and quantification (right) of YL-mediated suppression of c-Fos immunolabeling in the MCC evoked by capsaicin injection into the lower hind leg in mice expressing ArchT in the contralateral MCC ($n = 3$ mice per group; $U_{left} = 32.5$, $P < 0.001$; $U_{right} = 30.5$, $P < 0.001$; "Left," cortex ipsilateral to stimulation; "Right," cortex contralateral to stimulation). Indicated are ArchT-expressing cells (green) positive (unfilled arrowheads) or negative (filled arrowheads) for Fos (red). Nuclei are shown with DAPI (blue). Scale bars, 100 µm. (**g**) Mechanical withdrawal frequencies to von Frey filament application upon YL-mediated silencing of the contralateral MCC ($n = 5$; $F_{(1,4)} = 0.47$, $P = 0.53$), S1HL ($n = 8$; $F_{(1,7)} = 2.61$, $P = 0.15$) or both MCC and S1HL ($n = 6$; $F_{(1,5)} = 41.29$, $P = 0.001$). Data in **g** shown as mean ± s.e.m. In **c** and **f**, box limits define the 25th and 75th percentiles, cross lines indicate the median and whiskers define the 10th and 90th percentiles. $^*P < 0.05$, Mann–Whitney test. In **g**, $^*P < 0.05$ compared to baseline, two-way repeated measures ANOVA with Bonferroni multiple comparison. *P* values in figure lettering represents significance between the entire stimulus curve compared to the control curve; n.s., not significant.

(**Fig. 1f** and **Supplementary Fig. 4**), which was used to identify the optimal optic fiber position for optogenetic silencing of the MCC. When we blocked neuronal activity by tonic photoactivation of virally transduced ArchT over the 15–30 min after capsaicin injection, the number of c-Fos-expressing cells in the MCC was significantly and markedly reduced (**Fig. 1f** and **Supplementary Fig. 4b**). Despite efficient inhibition of the MCC, capsaicin-evoked acute nocifensive behaviors, such as scratching, licking, flicking or lifting the injected hindpaw, which reflect both sensory and negative affective components of acute pain, were not suppressed within the photosilencing period (**Supplementary Fig. 5a**). This was also true for experiments involving ArchT-mediated silencing of the hind limb representation area in the somatosensory S1 cortex (S1HL) (**Supplementary Fig. 5a**), which receives strong spinothalamic nociceptive input in parallel to the MCC. Notably, simultaneous silencing of the MCC and S1HL *in vivo* using a dual fiber approach also did not affect capsaicin-evoked nocifensive behavior (**Supplementary Fig. 5a**), suggesting redundancy between these primary target sites of thalamocortical nociceptive input and other cortical and subcortical pathways in sensory and affective dimensions of capsaicin-evoked acute pain.

Similarly, acute withdrawal behavior of the hindpaw triggered by plantar application of graded mechanical stimuli (von Frey filaments) was independent of ArchT-mediated tonic silencing of either the MCC or S1HL (**Fig. 1g** and **Supplementary Fig. 5b**,**c**). Illumination of control-implanted mice, as well as mice expressing GFP under the *Camk2a* promoter, did not lead to changes in mechanical response frequency or threshold (**Supplementary Fig. 6a**,**b**). Surprisingly, simultaneous silencing of the MCC and S1HL paradoxically enhanced sensitivity to noxious and innocuous mechanical stimuli (**Fig. 1g**), an effect that was temporally locked to the duration of the yellow light illumination and did not persist thereafter (**Supplementary Fig. 5b**).

© 2017 Nature America, Inc., part of Springer Nature. All rights reserved.

© 2017 Nature America, Inc., part of Springer Nature. All rights reserved.

This observation suggests that the MCC and S1 cooperatively participate in tonic modulation of pathways inhibiting pain.

We then interrogated the functions of MCC and S1HL in a model of nociceptive activity-induced central plasticity. In humans and rodents[20,21], intense C-fiber nociceptor activation by capsaicin not only evokes acute pain and sensitization in the injected area, but also elicits a long-lasting sensitization to noxious and innocuous stimuli in neighboring dermatomes that were not exposed to capsaicin. Maintenance of this C-nociceptor-induced secondary hypersensitivity is largely independent of ongoing peripheral inputs and serves as a model for mechanisms of acquisition and maintenance of pain-related memory processes and central plasticity[20,21]. Using independent cohorts of rAAV-injected mice, we observed that activity of the MCC and S1HL was necessary for the induction of C-nociceptor-induced central plasticity. When either the MCC or S1HL were continuously silenced during mechanical testing of the paw over the 15–30 min after capsaicin injection in the lower hind leg region, the induction of mechanical hypersensitivity was blocked (**Fig. 2a** and **Supplementary Fig. 6**). However, when tested 45–60 min after capsaicin, control implanted mice (animals receiving optic fiber implantations only) and S1HL-silenced mice showed marked hypersensitivity, whereas MCC-silenced mice did not (**Fig. 2a** and **Supplementary Fig. 7a**,**b**). This suggests that ongoing excitation in central circuits is operational in maintaining nociceptive hypersensitivity and that neurons in the MCC, but not the S1HL cortex, contribute to the persistent phase of this process.

When we intermittently silenced MCC activity exclusively over the period of application of the von Frey filaments to the hindpaw, instead of inhibiting it tonically over the entire 15 min testing period as in the above experiments, we observed a blockade of hypersensitivity at 15–30 min but a full recovery of long-lasting hypersensitivity at 45–60 min (**Fig. 2a**). This suggests that stimulus-independent, background ongoing activity in MCC neurons is important for long-lasting excitation in cortical circuits related to nociceptive sensitization. In support, *in vivo* electrophysiological recordings revealed increased ongoing activity in the MCC when tested 15–30 min after capsaicin, a time when behavioral sensitization becomes evident (**Fig. 2b** and **Supplementary Fig. 7c**).

To explore the influence of ongoing excitatory activity in the MCC on nociceptive activity-induced central plasticity, we silenced the MCC at different phases after capsaicin. Silencing MCC activity over 0–15 min, the period of nociceptor activation by capsaicin, entirely prevented mechanical hypersensitivity at 15–30 min, consistent with a direct and acute recruitment of MCC neurons by incoming nociceptive activity and a role in acquisition of a sensitized state (**Fig. 2c**); these mice, however, still developed some mechanical sensitization at 45–60 min, albeit to a significantly lower degree than control implanted mice (**Fig. 2c** and **Supplementary Fig. 8a**,**b**). To address whether this results from ongoing excitation in the MCC, we silenced MCC activity in ArchT-expressing mice only over the period 30–45 min after capsaicin and found significantly reduced long-lasting mechanical hypersensitivity at 45–60 min (**Fig. 2c** and **Supplementary Fig. 8a**,**b**). Conversely, in mice expressing both ArchT and ChR2 within the same excitatory neurons of the MCC (**Supplementary Fig. 8c**), optogenetic stimulation of the same MCC neurons by blue light (473 nm; BL) over 45–60 min significantly enhanced nociceptive sensitivity in mice that had previously undergone MCC silencing over the 15–30 min after capsaicin, similarly to a retrieval of memory processes (**Fig. 3a** and **Supplementary Fig. 8d**). Taken together, these results suggest that ongoing activity in MCC neurons during different temporal phases after an acute peripheral barrage of C-fiber activity is obligatory for the induction and maintenance of central plasticity that is associated with a hypersensitivity response. We then tested whether acutely silencing the MCC could reverse established, long-lasting hypersensitivity. In a model of long-lasting inflammatory pain induced by hindpaw injection of complete Freund's adjuvant (CFA), yellow illumination of the MCC in ArchT-expressing mice 24 h after CFA partially, but significantly, attenuated mechanical hypersensitivity (**Fig. 3b**). In contrast, mechanical allodynia induced by peripheral neuropathy (the spared nerve injury model) was largely unaffected by acute silencing of the MCC (**Fig. 3c**–**e**), indicating a selective role of the MCC in persistent pain states that are driven and maintained by nociceptive inflow into the CNS.

All scenarios tested in the experiments above were entirely dependent on strong nociceptor afferent drive from the periphery, which activates the MCC and several other brain centers. We therefore tested whether MCC activation itself is sufficient to trigger behavioral plasticity. Whole-cell recordings over a period of 15 min in the MCC of cortical slices from mice expressing rAAV-encoded ChR2 revealed a consistent activation of pyramidal neurons with a high fidelity proportionally to graded blue illumination strength over the entire 15 min period of illumination, without any acute toxicity (**Fig. 4a** and **Supplementary Fig. 9**). MCC neurons showed significantly higher number of action potentials at frequencies of 20 Hz and 30 Hz as compared to 10 Hz (**Fig. 4a** and **Supplementary Fig. 9**). Using the same protocol in awake rAAV-Camk2a-ChR2-expressing mice, we observed a strong increase in the number of c-Fos-expressing neurons in both the ipsilateral and the contralateral MCC, as expected from the strong callosal connections (**Fig. 4b**). Using this protocol to elicit tonic activation of the MCC during mechanical von Frey filament stimulation of the paw in the absence of intraplantar capsaicin, we observed a marked hypersensitivity similar to that evoked by peripheral nociceptor drive; this became evident as a decrease in the response threshold to mechanical stimulation in both ipsilateral and contralateral hindpaws upon stimulation at 20 or 30 Hz (**Fig. 4c** and **Supplementary Fig. 10a**,**b**), consistent with the action potentials generated (**Fig. 4a**). This hypersensitivity lasted for several hours after a single illumination session (**Supplementary Fig. 10c**). In the same animals, stimulation of the MCC was not associated with negative affect in the conditioned place aversion test (**Fig. 4d**), and mice expressing neither ChR2 nor GFP in the MCC showed conditioned place aversion to the stimulation-paired context upon blue illumination (**Fig. 4d**). In contrast, and consistent with reports on negative affect elicited by glutamatergic stimulation of the rACC[9], we observed that, in mice expressing ChR2 in the rACC, blue illumination led to conditioned place aversion toward the stimulation-paired chamber as compared to the unconditioned chamber (**Fig. 4d**).

Next we aimed to unravel the nature of MCC-driven circuits involved in central plasticity. Using our mouse models with bidirectional modulation of nociceptive hypersensitivity via MCC silencing and MCC stimulation, we analyzed expression patterns of the activity-induced immediate early gene product c-Fos in the brains of mice with and without ChR2-mediated direct MCC activation and in capsaicin-injected mice with and without ArchT-mediated silencing of the MCC (**Fig. 5a**). Among the ten brain regions studied here (which have been associated with pain perception in human imaging experiments), only the nucleus accumbens (NAc), the posterior insula (PI) and an adjoining region, the claustrum, showed bidirectional modulation of c-Fos induction in line with bidirectional changes in nociceptive hypersensitivity upon MCC activation (via ChR2 in the absence of capsaicin) or MCC silencing (via ArchT in conjunction with hindpaw capsaicin injection) (**Fig. 5a** and **Supplementary Fig. 11**). Schematic

overviews of pain-related brain regions showing prominent changes in c-Fos expression upon MCC activation in the absence of capsaicin or MCC silencing in conjunction with peripheral capsaicin treatment are given in **Figure 5b**,**c**; examples are shown in **Figure 5d** and

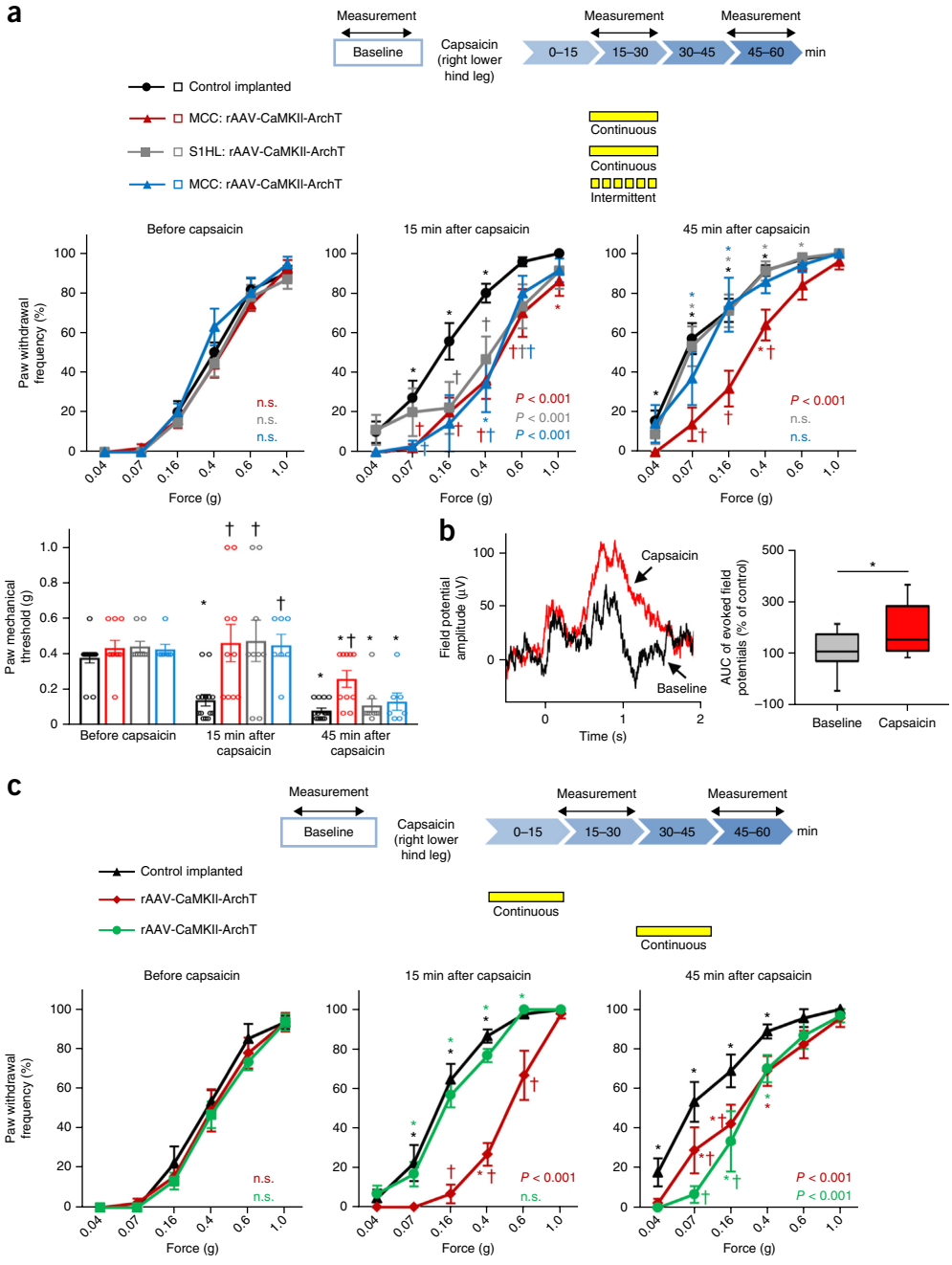

Figure 2 Activity in the MCC, not in S1HL, is necessary for centrally mediated, long-lasting nociceptive hypersensitivity. (**a**) Effects of yellow-light-mediated silencing of the MCC or S1HL on capsaicin-evoked secondary mechanical hyperalgesia to von Frey filament application on the contralateral paw. Top: schematic outline. Middle: impact of continuous yellow light (15 min) or intermittent yellow light (restricted to duration of von Frey application) ($n = 14$ for control group in black, $n = 10$ for MCC ArchT group in red, $n = 9$ for S1HL ArchT group in gray, $n = 7$ for MCC ArchT group in blue; pre-capsaicin: $F_{(3,15)} = 1.58$, $P = 0.196$; 15 min: $F_{(3,15)} = 14.9$, $P < 0.001$; 45 min: $F_{(3,15)} = 18.82$, $P < 0.001$). Bottom: mechanical thresholds. (**b**) Left: averaged field potential traces evoked by noxious von Frey stimulation (20 trials before and after capsaicin, $n = 4$ mice; $U = 1{,}758$, $P < 0.001$). Right: area under the curve (AUC) from von Frey stimulation-evoked field potentials in the MCC before and 15 min after hind leg capsaicin injection, normalized to baseline. (**c**) Impact of silencing MCC activity over the induction phase or just before the measurement of the late phase of capsaicin-evoked mechanical hypersensitivity in mice ($n = 9$ for control group in black triangles, $n = 9$ for ArchT group in red diamonds, $n = 6$ for ArchT group in green circles; pre-capsaicin: $F_{(2,10)} = 1.087$, $P = 0.34$; 15 min: $F_{(2,10)} = 54.165$, $P < 0.001$; 45 min: $F_{(2,10)} = 14.893$, $P < 0.001$). Data shown as mean ± s.e.m. In **a** and **c**, $^{*}P < 0.05$ compared to baseline, $^{\dagger}P < 0.05$ compared to control group, two-way ANOVA with Bonferroni multiple comparison; color-coded P values represents significance between the entire stimulus curve compared to the control curve; n.s., not significant. In **b**, box limits define the 25th and 75th percentiles, cross lines indicate the median and whiskers define the 10th and 90th percentiles. $^{*}P < 0.05$, Mann–Whitney test.

© 2017 Nature America, Inc., part of Springer Nature. All rights reserved.

Supplementary Figure 12. Of note, we observed changes in activity of the medial thalamus neither upon MCC activation nor upon capsaicin treatment with and without MCC silencing (**Supplementary Fig. 13**). Surprisingly, although the basolateral amygdala was observed to structurally receive afferents from excitatory neurons in the MCC in our tracing experiments using eYFP-tagged ChR2 (**Fig. 5e**), we did

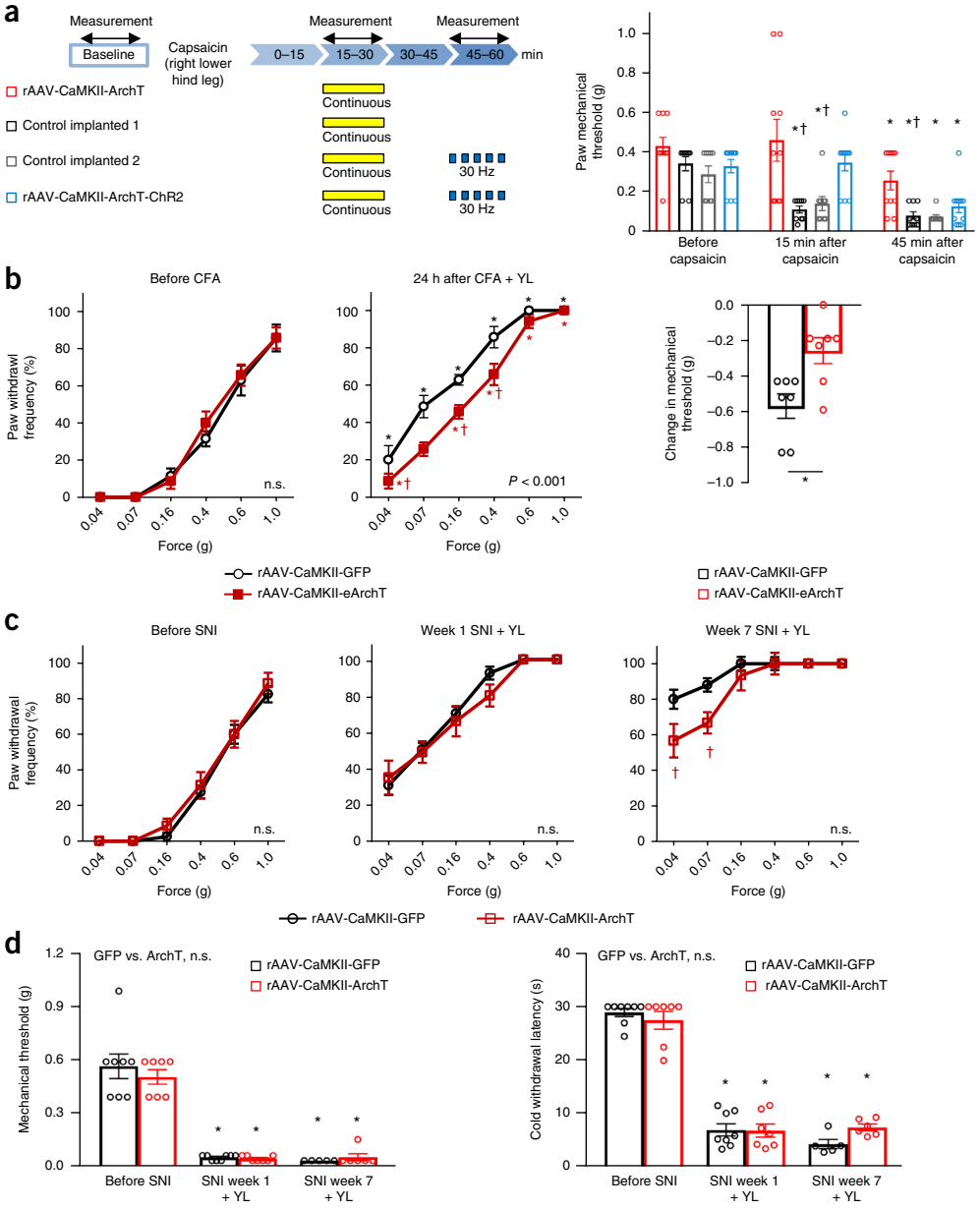

Figure 3 MCC activity plays a role in centrally mediated nociceptive hypersensitivity in acute persistent but not chronic nociception. (**a**) ArchT-mediated suppression of capsaicin-evoked mechanical hypersensitivity can be partially reversed by direct ChR2-mediated excitation of MCC neurons at 30 Hz over the subacute phase. Right: 40% mechanical thresholds ($n = 10$ for ArchT group, $n = 9$ for each control group, $n = 11$ for ArchT-ChR2 group; groups $F_{(3,6)} = 9.874$, $P < 0.001$; treatment $F_{(2,6)} = 27.502$, $P < 0.001$; groups × treatment $F_{(6,70)} = 2.639$, $P = 0.023$). (**b**) CFA-induced mechanical hypersensitivity is attenuated upon MCC photoinhibition 24 h after CFA ($n = 7$ per group; pre-CFA: $F_{(1,5)} = 0.115$, $P = 0.735$; 24 h: $F_{(1,5)} = 23.581$, $P < 0.001$). Right: change in 60% mechanical thresholds over baseline ($U = 6.5$, $P = 0.017$). YL, yellow light. (**c**) Mechanical allodynia induced by SNI remains largely the same between GFP and ArchT groups upon MCC photoinhibition at week 1 and week 7 after SNI ($n = 8$ for GFP, $n = 7$ for ArchT; pre-SNI groups $F_{(1,5)} = 1.248$, $P = 0.267$; week 1 groups $F_{(1,5)} = 0.683$, $P = 0.411$; week 7 groups $F_{(1,5)} = 4.406$, $P = 0.05$), although significant differences were observed at week 7 with respect to low intensity stimulation. (**d**) No differences in the 40% mechanical thresholds were observed before SNI and during MCC photoinhibition after SNI between GFP and ArchT groups ($F_{(1,2)} = 0.405$, $P = 0.529$). (**e**) SNI-induced cold allodynia in these animals was also unaffected upon MCC photoinhibition ($F_{(1,2)} = 0.298$, $P = 0.589$). Data shown as mean ± s.e.m. $^{*}P < 0.05$ compared to respective baseline (in **a**,**b**), $^{\dagger}P < 0.05$ compared to control group (black in **a**,**b**) or GFP control group (in **c**), $^{*}P < 0.05$ compared to respective pre-SNI values (**d**,**e**). Two-way repeated measures ANOVA with Bonferroni multiple comparisons was performed in **a**,**d**,**e**; two-way ANOVA with Bonferroni multiple comparisons in **b** (left) and **c**; Mann–Whitney test in **b** (right). *P* values in figure represents significance between the entire stimulus curve compared to the control curve or differences between GFP and ArchT groups; n.s., not significant.

© 2017 Nature America, Inc., part of Springer Nature. All rights reserved.

© 2017 Nature America, Inc., part of Springer Nature. All rights reserved.

not observe specific MCC-driven c-Fos expression in the amygdala (**Fig. 5a**). Along these lines, capsaicin-induced c-Fos expression in the prefrontal prelimbic and infralimbic cortices, which are believed to be anatomically connected with the MCC, was nearly completely suppressed by silencing of the MCC. However, direct photostimulation of the MCC did not yield significant c-Fos expression in prelimbic and infralimbic cortices (**Supplementary Fig. 11**), suggesting a more complex or indirect nature of the connectivity. Similarly, the anterior insula, S1HL and central amygdaloid nucleus did not show bidirectional changes in c-Fos expression corresponding to MCC inhibition and activation (**Supplementary Fig. 11**), indicating the importance of comparing at least two different models when circuits for a given behavior need to be identified by c-Fos mapping. Thus, only the PI and the NAc showed bidirectional changes in c-Fos expression that matched with high fidelity to bidirectional changes in MCC activity. Therefore, although we do not rule out contributions of other regions, we hypothesize that efferent projections from the MCC to the PI and NAc influence nociceptive plasticity and the induction of nociceptive hypersensitivity. Indeed, MCC–NAc projections can be visualized by virus-mediated expression of *Camk2a* promoter–driven eYFP-tagged ChR2 in excitatory neurons in the MCC (**Fig. 5e**). Additionally, we report here a previously undescribed excitatory axonal pathway from excitatory neurons of the MCC to layer 2/3 of the PI (**Fig. 5e**).

To further investigate whether the activated MCC-to-PI and MCC-to-NAc projections are functionally involved in the induction of nociceptive hypersensitivity, we directly stimulated or inhibited the MCC projections to the PI or the NAc using optogenetic manipulations. First, we unilaterally infected MCC neurons with a rAAV expressing an improved variant of ArchT, eArchT[22]. We then photosilenced eArchT-expressing projections via an optic fiber placed in the target region (PI or NAc) during behavioral testing 15–30 min after MCC activation by capsaicin injection in the contralateral lower hind leg (**Fig. 6a**). Unilaterally silencing the MCC-to-NAc projections affected mechanical hypersensitivity in the contralateral hindpaw during the early response phase to a small extent only and did not show an effect when tested during the late phase (**Fig. 6a**). As compared to illumination in mice expressing GFP, unilateral yellow illumination of the MCC-to-PI projection in eArchT-expressing mice significantly inhibited mechanical hypersensitivity in the contralateral hindpaw, not only at 15–30 min after capsaicin but also at 45–60 min (**Fig. 6b**), in a manner reminiscent of the behavioral consequence of MCC silencing in the capsaicin experiments described above. Inhibition of axon terminals using ArchT has been paradoxically linked to increased neurotransmitter release in some systems[23]. Therefore, in another set of mice, we directly silenced the target zone of the MCC-to-PI pathway—namely, PI neurons—and observed a similar inhibition of capsaicin-induced mechanical hypersensitivity (**Fig. 6b**). No changes were found in baseline nociceptive sensitivity upon silencing either the MCC-to-PI projections or the PI in the absence of capsaicin-evoked C-fiber stimulation (**Supplementary Fig. 14a,b**). Thus, inhibition of the PI recapitulated the main phenotypic changes elicited by inhibition of the MCC-to-PI projections.

In the second approach, we directly photoactivated the MCC-to-PI and MCC-to-NAc afferent projections by virally expressing ChR2 in excitatory neurons in the MCC and placing the optic fiber in the projection area—the PI or NAc, respectively (**Fig. 7a**). As compared to that in mice expressing GFP alone, blue illumination of the ChR2-expressing MCC-to-PI projection, but not of the ChR2-expressing MCC-to-NAc projection, induced significant mechanical hypersensitivity in the absence of hindpaw capsaicin injection (**Fig. 7a**). Thus, direct stimulation of MCC projections to the PI, but not MCC projections to the NAc, largely recapitulated the hypersensitivity that we observed upon stimulating excitatory neurons in the MCC.

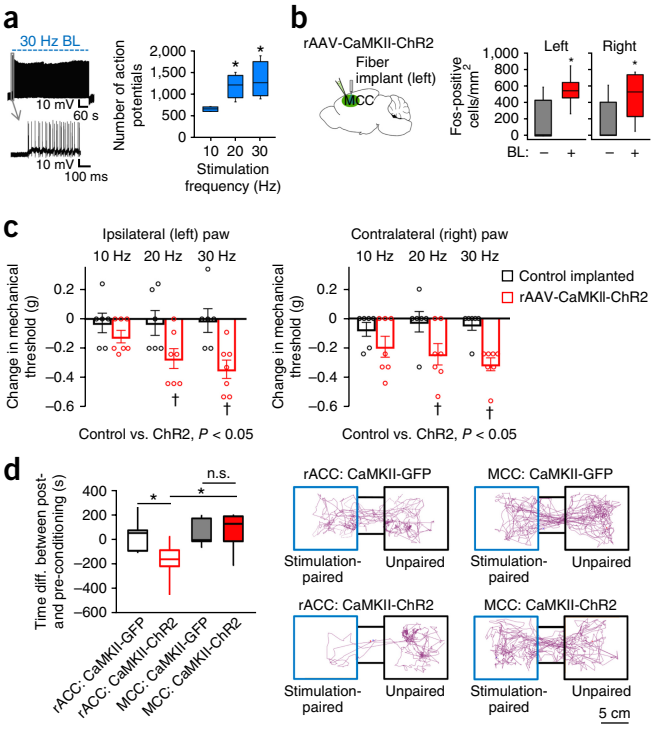

Figure 4 MCC activity plays a role in centrally mediated nociceptive hypersensitivity but not negative affect. (**a**) Example of a whole-cell recording with 30-Hz stimulation of ChR2 via blue light (BL). Gray box indicates time frame of response shown at a higher temporal resolution below. The number of action potentials during a 30-s stimulation increases with the stimulation frequency ($n = 4$ cells from 3 mice per group, $F_{(2,9)} = 5.894$, $P = 0.023$). (**b**) Quantification of Fos immunolabeling indicating activation of MCC neurons upon BL *in vivo* in the left (ipsilateral to stimulation) and right (contralateral to stimulation) cortex (left: $n = 19$ and 17 samples in the absence and presence of BL, respectively, $U = 45$, $P < 0.001$; right: $n = 18$ and 16 samples in the absence and presence of BL, respectively, $U = 50.5$, $P = 0.001$; from 4 mice). (**c**) Mechanical thresholds of the hindpaws were reduced compared to baselines in MCC-stimulated animals ($n = 6$) with increasing stimulation frequencies (10, 20 and 30 Hz) compared to those in control animals ($n = 7$; ipsilateral: $F_{(1,2)} = 6.359$, $P = 0.028$, contralateral: $F_{(1,2)} = 8.131$, $P = 0.016$). (**d**) Left: time difference spent in the conditioned chamber (after vs. before conditioning) in mice with photostimulation in the rACC or MCC ($n = 7$ mice per group; $F_{(3,24)} = 5.19$, $P = 0.007$). Right: example track plots from mice after conditioning; area highlighted in blue indicates the light-paired chamber. Avoidance of chamber is present in rACC-conditioned mice, but not in MCC-conditioned or control GFP-injected animals. $^{*}P < 0.05$ compared to respective baseline, $^{\dagger}P < 0.05$ compared to control group (black), two-way ANOVA with repeated measures (**c**) or one-way ANOVA (**a**,**d**) with Bonferroni multiple comparison, Mann–Whitney test in **b**. Data in **c** shown as mean ± s.e.m.; box limits define the 25th and 75th percentiles, cross lines indicate the median and whiskers define the 10th and 90th percentiles.

Motor function and locomotion were not affected by modulating MCC-to-PI or the MCC-to-NAc projections, indicating that the above behavioral readouts were not confounded by overt disturbances in motor function (**Fig. 7b**). Notably, in the open field test, we did not observe any modulation of fear-related behavior (thigmotaxis, center-to-margin ratio) upon stimulating or inhibiting the MCC-to-PI or the MCC-to-NAc projections using the same parameters as

© 2017 Nature America, Inc., part of Springer Nature. All rights reserved.

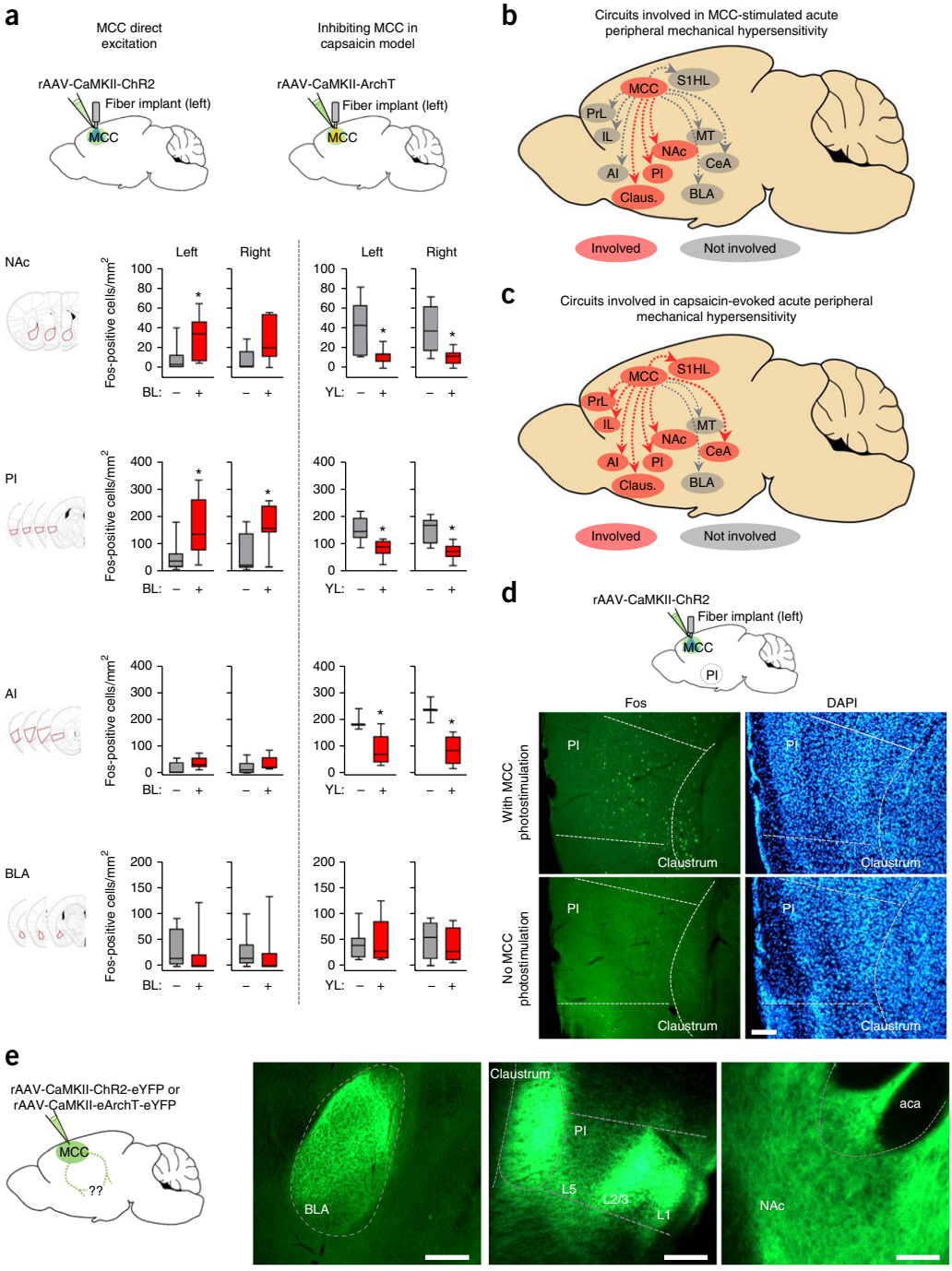

Figure 5 Functional and structural mapping of MCC target regions in the context of sensory modulation. (**a**) Analysis of Fos-positive cells as a marker for neuronal activation in diverse brain regions of mice with optogenetic activation of the MCC or mice with MCC silencing during capsaicin-evoked mechanical hypersensitivity in the absence or presence of photostimulation in the left (ipsilateral to stimulation) and right (contralateral to stimulation) cortex (blue light (BL) for ChR2-mediated activation and yellow light (YL) for ArchT-mediated silencing; $n = 3$ mice for NAc, BL: $t_{left} = -2.709$, d.f. = 15, $P = 0.0162$; $t_{right} = -1.907$, d.f. = 11, $P = 0.083$; YL: $U_{left} = 20$, $P = 0.017$, $U_{right} = 7$, $P = 0.007$; $n = 5$ mice for PI, BL: $U_{left} = 31$, $P = 0.007$, $U_{right} = 21$, $P = 0.021$; YL: $t_{left} = 5.538$, d.f. = 34, $P = 0.00000344$; $t_{right} = 5.502$, d.f. = 29, $P = 0.0000063$; $n = 3$ for anterior insula (AI), BL: $U_{left} = 16$, $P = 0.189$, $U_{right} = 13$, $P = 0.354$; YL: $t_{left} = 3.073$, d.f. = 9, $P = 0.013$, $t_{right} = 2.961$, d.f. = 4, $P = 0.0415$; $n = 3$ for basolateral amygdala (BLA), BL: $U_{left} = 15.5$, $P = 0.395$, $U_{right} = 17.5$, $P = 0.414$; YL: $U_{left} = 63$, $P = 0.878$, $t_{right} = 0.638$, d.f. = 10, $P = 0.538$). (**b**,**c**) Schematic representation of MCC target areas that emerged from the above-described experiment. Red shading: regions involved; gray shading: regions not involved. Arrows do not necessarily indicate direct point-to-point connections; these connections may also occur indirectly via one of the highlighted nuclei (red and gray). PrL, prelimbic cortex; IL, infralimbic cortex; AI, anterior insula; Claus., claustrum; MT, medial thalamus; CeA, central amygdaloid nucleus; BLA, basolateral amygdala. (**d**) Typical example of changes in Fos expression in the PI and claustrum upon optogenetic stimulation of the MCC (scale bar, 100 µm). (**e**) Examples of viral tracing of projections of MCC excitatory neurons expressing ArchT- or ChR2-tagged eYFP under control of the *Camk2a* promoter to the basolateral amygdala (BLA; scale bar, 500 µm), claustrum, PI and NAc ($n = 4$ mice; scale bars, 200 µm); aca, anterior commissure anterior part. Box limits define the 25th and 75th percentiles, cross lines indicate the median and whiskers define the 10th and 90th percentiles. $^*P < 0.05$, Mann–Whitney test.

described above (**Fig. 7b**). Freezing behaviors were also absent in all animals. This indicates that MCC-triggered fear responses described previously[2,3] do not involve the MCC-to-PI projections.

Finally, we sought to address whether the MCC and the MCC–PI pathway bring about sensitization of nociceptive behaviors exclusively via supraspinal mechanisms or whether they act on spinal nociceptive processing via descending modulation. We stimulated ChR2-expressing MCC neurons or the MCC projections in the PI at 30 Hz, as described above (**Fig. 4**), in mice that were intrathecally (i.t.) injected with the drug granisetron[24], a blocker of descending serotonergic facilitation to the spinal cord. Optogenetic activation of the MCC or the MCC–PI pathway evoked pronounced hypersensitivity in ChR2-expressing mice receiving blue illumination, but not in mice that also received i.t. granisetron treatment (**Fig. 7c**). This suggests a strong downstream contribution of descending serotonergic facilitation in the pronociceptive functions of the MCC, as well as the MCC–PI pathway. Administration of i.t. granisetron alone had no effect on basal mechanical sensitivity (**Fig. 7d**). To further address the links between the MCC–PI pathway and descending serotonergic facilitation, we injected rAAV expressing GFP in the PI. Confocal microscopy revealed that virally traced excitatory projections arising from the PI were prominent in the raphe magnus nucleus (**Fig. 7e** and **Supplementary Fig. 15**), the site of origin of descending serotonergic projections, thereby further supporting a role for descending

© 2017 Nature America, Inc., part of Springer Nature. All rights reserved.

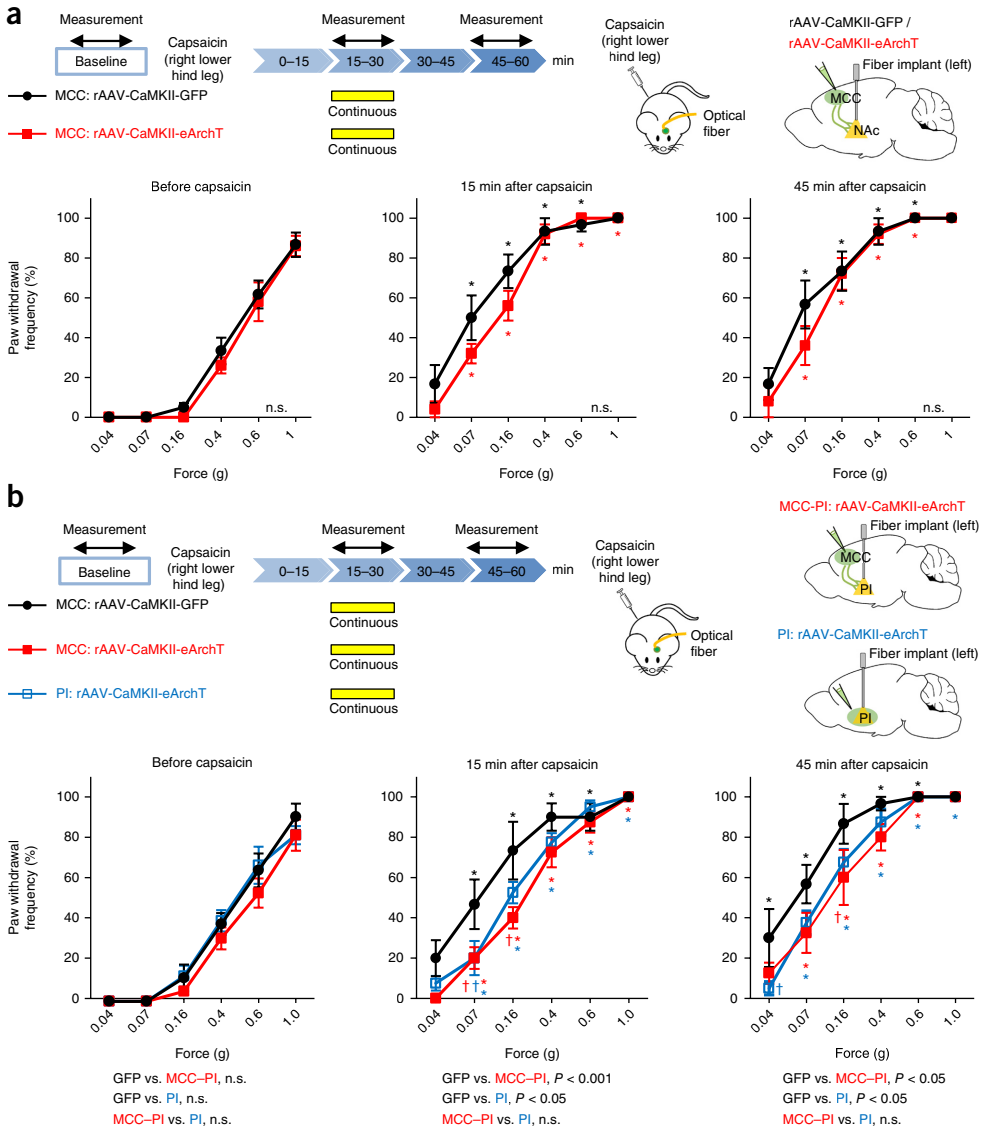

Figure 6 Impact of optogenetic silencing of the axonal projections from the MCC to the PI or NAc on basal nociception and capsaicin-evoked mechanical hypersensitivity. (**a**,**b**) Top panels: eArchT expression in MCC–PI or MCC–NAc projections and their photoinhibition. Bottom panels: behavioral influence of afferent silencing during the expression of early hypersensitivity continuously over the 15–30 min following contralateral hind leg injection of capsaicin (in **a**, $n = 6$ for MCC–NAc ArchT, $n = 5$ for MCC–NAc GFP, pre-capsaicin: $F_{(1,5)} = 1$, $P = 0.322$; 15 min: $F_{(1,5)} = 3.358$, $P = 0.072$; 45 min: $F_{(1,5)} = 1.662$, $P = 0.208$; in **b**, $n = 8$ for MCC–PI ArchT, $n = 5$ for MCC–PI GFP, $n = 8$ for PI ArchT; pre-capsaicin: $F_{(2,10)} = 2.161$, $P = 0.12$; 15 min: $F_{(2,10)} = 10.4$, $P < 0.001$; 45 min: $F_{(2,10)} = 6.684$, $P = 0.002$). Data shown as mean ± s.e.m. Throughout the figure, $^{*}P < 0.05$ compared to respective baseline, $^{\dagger}P < 0.05$ compared to GFP group, two-way ANOVA with Bonferroni multiple comparison; color-coded P values in each panel represents significance between the entire stimulus curve compared to the control curve or as indicated; n.s., not significant.

© 2017 Nature America, Inc., part of Springer Nature. All rights reserved.

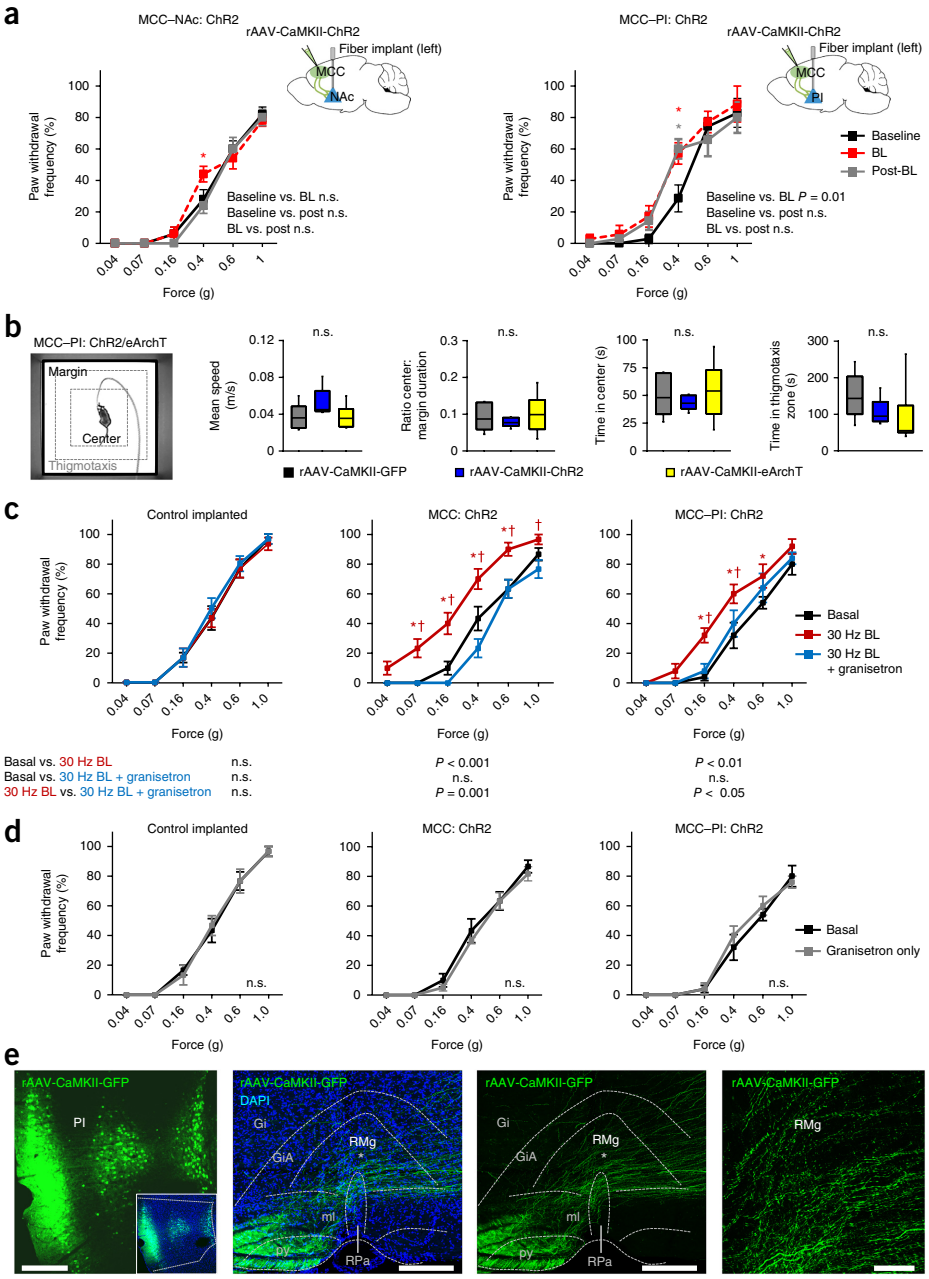

Figure 7 Optogenetic interrogation of the projections from MCC to PI or to NAc with respect to nociceptive plasticity, fear behavior and analysis of descending serotonergic facilitation. (**a**) Schematics of ChR2 expression and blue light (BL) photoactivation of afferents (30 Hz, ~40 mW/mm^2, 15 min) in the respective target regions and impact on mechanical sensitivity in the basal state (MCC–NAc: $n = 10$, $F_{(2,18)} = 1.465$, $P = 0.257$; MCC–PI: $n = 7$, $F_{(2,12)} = 5.342$, $P = 0.022$). (**b**) Impact of photosilencing or photoactivation of MCC–PI afferent projections on fear-related behavior in the open-field test ($n = 5$ each for GFP and ChR2, $n = 6$ for ArchT; speed: $H = 4.938$, $P = 0.09$; duration ratio: $H = 0.576$, $P = 0.75$; center: $H = 0.576$, $P = 0.75$; thigmotaxis: $H = 4.169$, $P = 0.124$; d.f. = 2 for all). (**c**) Effect of i.t.-injected granisetron on mechanical hypersensitivity induced in the contralateral paw by 30-Hz BL stimulation of either the MCC or the MCC–PI pathway (control: $n = 6$, $F_{(2,10)} = 0.443$, $P = 0.654$; MCC: ChR2: $n = 6$, $F_{(2,10)} = 25.297$, $P < 0.001$; MCC–PI: ChR2: $n = 5$, $F_{(2,8)} = 13.913$, $P = 0.002$). (**d**) Effects of i.t. granisetron alone on basal mechanical sensitivity in the absence of MCC or MCC–PI stimulation (control: $n = 6$, $F_{(1,5)} = 0.224$, $P = 0.656$; MCC: ChR2: $n = 6$, $F_{(1,5)} = 1.623$, $P = 0.259$; MCC–PI: ChR2: $n = 5$, $F_{(1,4)} = 0.385$, $P = 0.569$). (**e**) Examples of neuronal projections virally traced (green) from PI (far left; overlaid with DAPI in blue in inset) to the raphe magnus nucleus (RMg; asterisk) in central panels; scale bars, 250 µm. Gi, gigantocellular reticular nucleus; GiA, gigantocellular reticular nucleus, alpha part; ml, medial lemniscus; py, pyramidal tract; RPa, raphe pallidus nucleus. Far right: high magnification view of the RMg; scale bar 100 µm (details in **Supplementary Fig. 15**). $^*P < 0.05$ to respective baseline, $^\dagger P < 0.05$ to 30 Hz plus granisetron; two-way ANOVA repeated measures with Bonferroni multiple comparison (**a**,**c**), one-way ANOVA on ranks (**b**), two-way ANOVA with Bonferroni multiple comparison (**d**). *P* values in figure represents significance between each stimulus curve; n.s., not significant. Data in **a**,**c**,**d** shown as mean ± s.e.m.; box limits define the 25th and 75th percentiles, cross lines indicate the median and whiskers define the 10th and 90th percentiles (**b**).

facilitatory systems in mediating the influence of the MCC–PI pathway on nociception.

In summary, we identify a MCC-to-PI projection as a pathway for the induction and maintenance of nociceptive hypersensitivity downstream of C-fiber activation. Moreover, we provide experimental evidence that activation of the MCC-to-PI pathway is sufficient to induce nociceptive hypersensitivity in the absence of conditioning nociceptor inputs and that it functions to modulate pain independently of evoking stimulus-dependent fear or negative affect.

DISCUSSION

The specificity of functional divisions in subdomains of the cingulate cortex still remains unclear[2,3]. Although human neuroimaging studies on subdivisions of the ACC have yielded extensive correlations and strong predictive associations with pain, aversion, pain anticipation and fear, causal links have remained elusive owing to the lack of interventional manipulations[2,3]. Here, interrogative analyses using optogenetics to target specific cellular populations, as well as to map and manipulate circuits with temporal precision, revealed that the MCC domain gates sensory hypersensitivity, but not acute pain or affect-related behaviors in mice. Although not all neurons and subdomains over the entire MCC can be targeted simultaneously with optogenetics, manipulating activity of about 80% of the excitatory neurons within the illuminated region was sufficient to modulate nociceptive sensory plasticity, but not acute pain or affect. These findings call into question the popular view that the 'medial' nociceptive pathway targeting the cingulate cortex exclusively mediates the affective component of pain while the 'lateral' nociceptive pathway targeting the somatosensory cortex and insula selectively mediates nociception and plasticity of sensory processing, a dogma that is being increasingly challenged[25,26].

Rodent studies on the functions of the ACC in pain describe either an exclusive role in pain-related negative affect but not in the sensory component of pain[8–10] or pronociceptive sensory functions[11–16]. Most studies addressing the impact of cingulate function on nociception have targeted the pregenual ACC (rACC)[9,14,16,27–30], whereas we focused exclusively on the MCC, which is a cytoarchitecturally and functionally distinct subdomain of the cingulate across several species, including mouse, rat and human[7]. Our experimental approach based on targeting specific, functionally distinct subdivisions and elucidating circuit contributions enabled us to dissect different components of pain at a cellular network level. When our results on the MCC and rACC are taken together with two previous important studies selectively manipulating the rACC in rodents[9,10], a picture emerges suggesting that the ACC and the MCC domains mediate negative affective and sensory dimensions of pain sensitivity, respectively, which is consistent with predictions from some earlier and recent imaging studies on human subjects[1,18,31].

Our data show that while the S1 cortex and the MCC are important for induction of early behavioral plasticity with strong nociceptive input, only ongoing activity in excitatory neurons of the MCC influences the transition to a subacute maintenance of hypersensitivity after cessation of peripheral inputs. With respect to long-term plasticity in pathological pain states, we observed different contributions of the MCC to inflammatory pain and neuropathic pain. Although both of these chronic pain states involve central plasticity, it is widely acknowledged that their mechanisms and underlying pathways diverge considerably, not only with respect to the peripheral afferents involved but also in terms of participating central circuits[32]. Currently, glia-dependent mechanisms and circuits related to affect, emotions and reward are in prominent focus as determinants of neuropathic pain[32]. Our observation that acute silencing of the MCC can partially, but significantly, reverse inflammatory hypersensitivity offers a perspective on many clinical pain disorders that involve prominent participation of nociceptors and activity-dependent plasticity in nociceptor-driven flow in ascending pathways.

Notably, our experiments involving temporally restricted optogenetic control of MCC activity, as well as c-Fos-based mapping of brain regions that were modified in activity by MCC silencing or activation, show that the MCC is a key locus connected in circuits mediating a hypersensitive state and provide functional evidence that the MCC functions in the rapid behavioral adaptive control in response to threat that has been predicted by some imaging studies in humans[3,33]. We observed that the MCC-associated network spans several cortical and subcortical regions based on c-Fos activity maps, including other regions in the prefrontal cortex that have recently shown to regulate central pain processing[34,35]. However, the most clear-cut functional associations found in our analyses were between the MCC and the PI, NAc and claustrum.

In functional photosilencing and tracing experiments, we identified a previously undescribed pathway linking excitatory neurons in the MCC to layer 2/3 neurons in the PI, which we found to be sufficient to induce and maintain a hypersensitive state. There are diverse views on the contributions of the anterior insula and PI to pain perception and processing[2,36–38]. According to Craig's model, the PI generates the initial cortical representation of the body's homeostatic condition that then provides the anterior insula information upon which emotions associated with that representation are generated[36]. Reports that physical intensity of a pain stimulus correlates with activation in the PI in human subjects, whereas perceived pain correlates with activation in the bilateral anterior insula[36], would be consistent with the function we observed here for connectivity to the PI in sensory hypersensitivity.

We have not determined here how sensory hypersensitivity is gated by the MCC and the MCC-to-PI pathway. Several mechanisms are possible, such as modulation of an anticipatory network (which involves the MCC but not the rACC[39]), influence on attention[40], modulation of the 'salience network' (which involves the MCC as a node[41]), modulation of ascending spinothalamic and thalamocortical nociceptive inputs into the PI[2] or regulation of spinal nociceptive processing via descending control pathways, as discussed below. The MCC is also anatomically related to cingulate premotor areas, which are hypothesized to directly govern adaptive motor responses to threatening stimuli[2], and recent studies suggest a close overlap between MCC regions activated during pain and motor control[42]. Also noteworthy are the multiple lines of evidence linking the PI to intensity coding, including pain intensity encoding[37], and it has been proposed that the insula subserves a general function as a 'how much' general magnitude detector[43]. Therefore, MCC-to-PI connections may harness this function of the PI in amplifying perception in the context of nociception. One notable mechanistic aspect revealed by this study is that, independently of which of the above supraspinal mechanisms participate following MCC activation, the final downstream process via which the MCC modulates nociceptive hypersensitivity is given by descending facilitation of spinal nociceptive processing. Indeed, we observed the PI to be anatomically and functionally connected with the raphe magnus nucleus, the site of origin of serotonergic modulation, and found that the MCC–PI pathway influenced nociception by recruiting descending serotonergic mechanisms. Serotonergic pathways originating in the raphe magnus nucleus exert prominent facilitatory modulation in the spinal cord, and optogenetic activation of brainstem serotonergic neurons has been recently reported to induce nociceptive hypersensitivity[44].

It is a matter of debate whether cortical plasticity is a mere reflection and manifestation of activity-dependent sensitization phenomena that

© 2017 Nature America, Inc., part of Springer Nature. All rights reserved.

have already taken place in the initial segments of the nociceptive pathway or whether structural and functional plasticity in the cortex can causally underlie pathological pain[45]. Here we report that activation of MCC-to-PI afferents alone can generate a state of nociceptive hypersensitivity independent of a peripheral nociceptive conditioning input. This has implications for changes in pain sensitivity reported in patients in the absence of (or persisting following healing of) obvious injuries or physical pathologies. Our data thus provide a mechanistic basis for exacerbation of pain by psychosocial factors that may deregulate basal activity in the MCC and the PI. Taken together, the results of the present study give insights into cortical circuitry involved in the transition from acute to persistent pain.

METHODS

Methods, including statements of data availability and any associated accession codes and references, are available in the online version of the paper.

Note: Any Supplementary Information and Source Data files are available in the online version of the paper.

ACKNOWLEDGMENTS

We thank R. LeFaucheur for secretarial help, as well as N. Gehrig, V. Buchert, L. Brenner, H.-J. Wrede, D. Baumgartl-Ahlert and K. Meyer for technical assistance. We are grateful to the Interdisciplinary Neurobehavioral Core Facility in Heidelberg for support with behavioral experiments. We gratefully acknowledge funding in form of SFB1158 grants from the Deutsche Forschungsgemeinschaft (DFG) to R.K. (project B01), T.K. (project B08), R.S. (project A05) and H.F. (project B07), European Research Council (ERC) Advanced Investigator grants to R.K. (Pain Plasticity 294293) and H.F. (Phantommind 230249) and DFG funding via the Excellence Cluster CellNetworks (Ectop funding to R.K. and H.F.). We acknowledge support from the European Molecular Biology Organization (EMBO) to L.L.T. in the form of an EMBO long-term postdoctoral fellowship.

AUTHOR CONTRIBUTIONS

L.L.T., R.S., H.F., T.K. and R.K. were involved in manuscript preparation. L.L.T. conducted the experiments and analyzed data. R.K. designed the study and wrote the manuscript. W.T. generated the viruses; V.G. helped with behavioral experiments; C.H. and P.P. performed electrophysiology experiments.

COMPETING FINANCIAL INTERESTS

The authors declare no competing financial interests.

Reprints and permissions information is available online at http://www.nature.com/reprints/index.html. Publisher's note: Springer Nature remains neutral with regard to jurisdictional claims in published maps and institutional affiliations.

1. Vogt, B.A., Berger, G.R. & Derbyshire, S.W.G. Structural and functional dichotomy of human midcingulate cortex. *Eur. J. Neurosci.* **18**, 3134–3144 (2003).
2. Vogt, B.A. Pain and emotion interactions in subregions of the cingulate gyrus. *Nat. Rev. Neurosci.* **6**, 533–544 (2005).
3. Shackman, A.J. *et al.* The integration of negative affect, pain and cognitive control in the cingulate cortex. *Nat. Rev. Neurosci.* **12**, 154–167 (2011).
4. Wager, T.D. *et al.* An fMRI-based neurologic signature of physical pain. *N. Engl. J. Med.* **368**, 1388–1397 (2013).
5. Xu, H. *et al.* Presynaptic and postsynaptic amplifications of neuropathic pain in the anterior cingulate cortex. *J. Neurosci.* **28**, 7445–7453 (2008).
6. Apps, M.A.J., Lockwood, P.L. & Balsters, J.H. The role of the midcingulate cortex in monitoring others' decisions. *Front. Neurosci.* **7**, 251 (2013).
7. Vogt, B.A. & Paxinos, G. Cytoarchitecture of mouse and rat cingulate cortex with human homologies. *Brain Struct. Funct.* **219**, 185–192 (2014).
8. Gao, Y.J., Ren, W.H., Zhang, Y.Q. & Zhao, Z.Q. Contributions of the anterior cingulate cortex and amygdala to pain- and fear-conditioned place avoidance in rats. *Pain* **110**, 343–353 (2004).
9. Johansen, J.P. & Fields, H.L. Glutamatergic activation of anterior cingulate cortex produces an aversive teaching signal. *Nat. Neurosci.* **7**, 398–403 (2004).
10. Qu, C. *et al.* Lesion of the rostral anterior cingulate cortex eliminates the aversiveness of spontaneous neuropathic pain following partial or complete axotomy. *Pain* **152**, 1641–1648 (2011).
11. Wei, F. *et al.* Genetic elimination of behavioral sensitization in mice lacking calmodulin-stimulated adenylyl cyclases. *Neuron* **36**, 713–726 (2002).
12. Li, X.Y. *et al.* Alleviating neuropathic pain hypersensitivity by inhibiting PKMζ in the anterior cingulate cortex. *Science* **330**, 1400–1404 (2010).
13. Koga, K. *et al.* In vivo whole-cell patch-clamp recording of sensory synaptic responses of cingulate pyramidal neurons to noxious mechanical stimuli in adult mice. *Mol. Pain* **6**, 62 (2010).
14. Kang, S.J. *et al.* Bidirectional modulation of hyperalgesia via the specific control of excitatory and inhibitory neuronal activity in the ACC. *Mol. Brain* **8**, 81 (2015).
15. Ren, L.Y. *et al.* Distinct roles of the anterior cingulate cortex in spinal and supraspinal bee venom-induced pain behaviors. *Neuroscience* **153**, 268–278 (2008).
16. Gu, L. *et al.* Pain inhibition by optogenetic activation of specific anterior cingulate cortical neurons. *PLoS One* **10**, e0117746 (2015).
17. Schweinhardt, P. & Bushnell, M.C. Pain imaging in health and disease—how far have we come? *J. Clin. Invest.* **120**, 3788–3797 (2010).
18. Hu, L. *et al.* The primary somatosensory cortex and the insula contribute differently to the processing of transient and sustained nociceptive and non-nociceptive somatosensory inputs. *Hum. Brain Mapp.* **36**, 4346–4360 (2015).
19. Tye, K.M. & Deisseroth, K. Optogenetic investigation of neural circuits underlying brain disease in animal models. *Nat. Rev. Neurosci.* **13**, 251–266 (2012).
20. Luo, C. *et al.* Presynaptically localized cyclic GMP-dependent protein kinase 1 is a key determinant of spinal synaptic potentiation and pain hypersensitivity. *PLoS Biol.* **10**, e1001283 (2012).
21. Meyer, R.A., Ringkamp, M., Campbell, J.N. & Raja, S.N. Peripheral mechanism of cutaneous nociception. in *Wall and Melzack's Textbook of Pain* (eds. McMahon, S.B. & Koltzenburg, M.) 3–34 (Elsevier Churchill Livingstone, 2006).
22. Mattis, J. *et al.* Principles for applying optogenetic tools derived from direct comparative analysis of microbial opsins. *Nat. Methods* **9**, 159–172 (2011).
23. Mahn, M., Prigge, M., Ron, S., Levy, R. & Yizhar, O. Biophysical constraints of optogenetic inhibition at presynaptic terminals. *Nat. Neurosci.* **19**, 554–556 (2016).
24. Kayser, V. *et al.* Mechanical, thermal and formalin-induced nociception is differentially altered in 5-HT1A–/–, 5-HT1B–/–, 5-HT2A–/–, 5-HT3A–/– and 5-HTT–/– knock-out male mice. *Pain* **130**, 235–248 (2007).
25. Frot, M., Mauguière, F., Magnin, M. & Garcia-Larrea, L. Parallel processing of nociceptive A-delta inputs in SII and midcingulate cortex in humans. *J. Neurosci.* **28**, 944–952 (2008).
26. Apkarian, A.V., Baliki, M.N. & Geha, P.Y. Towards a theory of chronic pain. *Prog. Neurobiol.* **87**, 81–97 (2009).
27. Chen, T. *et al.* Postsynaptic potentiation of corticospinal projecting neurons in the anterior cingulate cortex after nerve injury. *Mol. Pain* **10**, 33 (2014).
28. Calejesan, A.A., Kim, S.J. & Zhuo, M. Descending facilitatory modulation of a behavioral nociceptive response by stimulation in the adult rat anterior cingulate cortex. *Eur. J. Pain* **4**, 83–96 (2000).
29. Johansen, J.P., Fields, H.L. & Manning, B.H. The affective component of pain in rodents: direct evidence for a contribution of the anterior cingulate cortex. *Proc. Natl. Acad. Sci. USA* **98**, 8077–8082 (2001).
30. Tang, J. *et al.* Pavlovian fear memory induced by activation in the anterior cingulate cortex. *Mol. Pain* **1**, 6 (2005).
31. Singer, T. *et al.* Empathy for pain involves the affective but not sensory components of pain. *Science* **303**, 1157–1162 (2004).
32. Kuner, R. & Flor, H. Structural plasticity and reorganisation in chronic pain. *Nat. Rev. Neurosci.* **18**, 20–30 (2016).
33. Sheth, S.A. *et al.* Human dorsal anterior cingulate cortex neurons mediate ongoing behavioural adaptation. *Nature* **488**, 218–221 (2012).
34. Zhang, Z. *et al.* Role of Prelimbic GABAergic Circuits in Sensory and Emotional Aspects of Neuropathic Pain. *Cell Rep.* **12**, 752–759 (2015).
35. Lee, M. *et al.* Activation of corticostriatal circuitry relieves chronic neuropathic pain. *J. Neurosci.* **35**, 5247–5259 (2015).
36. Craig, A.D. How do you feel—now? The anterior insula and human awareness. *Nat. Rev. Neurosci.* **10**, 59–70 (2009).
37. Segerdahl, A.R., Mezue, M., Okell, T.W., Farrar, J.T. & Tracey, I. The dorsal posterior insula subserves a fundamental role in human pain. *Nat. Neurosci.* **18**, 499–500 (2015).
38. Davis, K.D., Bushnell, M.C., Iannetti, G.D., St Lawrence, K. & Coghill, R. Evidence against pain specificity in the dorsal posterior insula. *F1000Res.* **4**, 362 (2015).
39. Palermo, S., Benedetti, F., Costa, T. & Amanzio, M. Pain anticipation: an activation likelihood estimation meta-analysis of brain imaging studies. *Hum. Brain Mapp.* **36**, 1648–1661 (2015).
40. Brown, C.A. & Jones, A.K.P. A role for midcingulate cortex in the interruptive effects of pain anticipation on attention. *Clin. Neurophysiol.* **119**, 2370–2379 (2008).
41. Wiech, K. *et al.* Anterior insula integrates information about salience into perceptual decisions about pain. *J. Neurosci.* **30**, 16324–16331 (2010).
42. Misra, G. & Coombes, S.A. Neuroimaging evidence of motor control and pain processing in the human midcingulate cortex. *Cereb. Cortex* **25**, 1906–1919 (2015).
43. Baliki, M.N., Geha, P.Y. & Apkarian, A.V. Parsing pain perception between nociceptive representation and magnitude estimation. *J. Neurophysiol.* **101**, 875–887 (2009).
44. Cai, Y.Q., Wang, W., Hou, Y.Y. & Pan, Z.Z. Optogenetic activation of brainstem serotonergic neurons induces persistent pain sensitization. *Mol. Pain* **10**, 70 (2014).
45. Ringkamp, M. & Raja, S.N. A sore spot: central or peripheral generation of chronic neuropathic spontaneous pain? *Pain* **155**, 1189–1191 (2014).

© 2017 Nature America, Inc., part of Springer Nature. All rights reserved.

ONLINE METHODS

Animals. C57Bl6 male wild-type mice (25–30 g, 8–14 weeks old) were housed in groups of 2–4 per cage with food and water *ad libitum* on a 12 h light/12 h dark cycle. All experimental procedures were approved by and adhere to ethical guidelines set by the local governing body (Governmental Council in Karlsruhe, Germany; approval numbers 35-9185.81/G115/11 and G119/14) and were performed according to the German Animal Welfare Act: Regulation for the Protection of Animals Used for Experimental or Other Scientific Purposes (Animal Welfare Regulation Governing Experimental Animals (TierSchVersV).

Plasmid constructs and virus transduction. The 2.4-kb *Camk2a* promoter sequence[46] was cloned into pAAV-Syn-ChR2A-tDimer[47] between the MluI and EcoRI restriction sites to generate pAAV-CaMKII-ChR2A-tDimer. The ArchT sequence was amplified by PCR and subcloned with BglII and XhoI into the pAAV-Syn-NpHR2A-Venus to generate pAAV-Syn-ArchT2A-Venus. The ArchT2A-Venus coding region was released from the pAAV-Syn-ArchT2A-Venus vector and subcloned into pAAV-CaMKII-ChR2A-tDimer to generate the pAAV-CaMKII-ChR2A-ArchT2A-Venus plasmid using BamHI and BsrGI. The *Camk2a* promoter sequence was inserted between the MluI and EcoRI restriction sites of pAAV-Syn-ArchT2A-Venus to generate plasmid pAAV-CaMKII-ArchT2A-Venus.

Recombinant adeno-associated viruses (rAAVs) serotypes 1 and 2 were generated as previously described[47] and purified by AVB Sepharose affinity chromatography[48]. For each virus preparation, the genomic titer was determined by real-time PCR (1.0×10^{12}–6.0×10^{12} viral genomes (vg)/ml, TaqMan Assay, Applied Biosystems). The neurotropic serotype 1/2 was used to preferentially infect neuronal cells[49]. The rAAV-CaMKIIα-EGFP construct was used as a control.

The rAAV-CaMKII-hChR2(H134R)-EYFP and rAAV-CaMKII-eArchT3.0-EYFP (both serotypes 5, 4×10^{12}–5.2×10^{12} vg/ml) constructs were purchased from the University of North Carolina Vector Core (USA). Sequence information for both plasmids is available at http://web.stanford.edu/group/dlab/optogenetics/sequence_info.html.

Surgical procedures. *Viral delivery. In vivo* delivery of rAAVs was carried out in 8-week-old male C57Bl6 mice by stereotactic injections. Mice were deeply anesthetized with an intraperitoneal injection of fentanyl (0.05 mg/ml), medetomidine hydrochloride (1 mg/ml) and midazolam (5 mg/ml) mixture (4:6:16, 0.7 µL per gram body weight). Lidocaine (10%) was applied to the skin surface and a small craniotomy was made above the region of interest. The coordinates used relative to bregma were as follows: MCC (0.20 to 0.25 mm anterior, −0.25 mm lateral, 0.75 mm depth), S1HL (0.13 mm posterior, −1.85 mm lateral, 0.45 mm depth), posterior insula (0.34 mm posterior, −3.85 mm lateral, 2.05 mm depth), nucleus accumbens (1.10 mm anterior, −1.50 mm lateral, 3.40 mm depth, 10° angle) and rACC (1.18 mm anterior, −0.25 mm lateral, 1.01 mm depth), according to the mouse brain atlas[50]. The MCC coordinates targeted in this study correspond to caudal parts of the Cg1 and Cg2 (areas 24b′ and 24a′, respectively)[7,51] and are anatomically distinct from the rACC regions that have been frequently targeted in several studies[9,14,27,29]. A further anatomical description is provided in **Supplementary Figure 1**.

Cortical injection of the purified rAAVs (≤0.7 µL per injection) was delivered over a 20–30 min period per site of interest for diffusion of virus. A cannula or chronic optical fiber implant was inserted 4 µm above each target site and secured to the skull with dental cement and a screw. Animals were kept for at least 3–4 weeks for optimal *in vivo* viral expression before behavioral and electrophysiological experiments. The sites of injection and viral expression were confirmed at the end of all experiments; animals displaying incorrect expression sites were excluded from all analysis.

Spared nerve injury (SNI). Mice were placed under isoflurane anesthesia (2%) and the fur of the right thigh was shaved. An incision was made to the lateral skin surface of the thigh and through the biceps femoris muscle to expose the sciatic nerve and its branches (sural, common peroneal and tibial nerves). The common peroneal and tibial nerves were tightly ligated with a silk suture and a section of the nerve bundle (2–4 mm) was cut and removed distal to the ligation, leaving the sural nerve intact. The muscle and skin were subsequently sutured close and animals left to recover in a heated cage for 24 h. Behavioral testing was carried out 7 d after the operation.

Complete Freund's adjuvant (CFA). Animals were briefly anesthetized and injected intraplantarly in the right paw with 20 µL CFA (Sigma-Aldrich) to induce inflammation.

Acute intrathecal (i.t.) delivery of drugs. Mice were placed under isoflurane anesthesia (1.5%) and granisetron (7 µg in 10 µL, dissolved in saline; Tocris) was injected as previously described[52]. The dosage of granisetron was chosen from previous reports[24].

***In vivo* optical stimulation.** Mice were briefly anesthetized and an optic fiber (≤200 µm in diameter) was inserted through the cannula via an internal guide. Animals with chronic optical fiber implants were connected to optical patch cables (Thorlabs GmbH, Germany) coupled to a 473-nm or 589-nm laser (Shanghai Laser & Optics Century Co. Ltd, China). Yellow illumination (589 nm, continuous mode, ~40 mW/mm^2; ~80 mW/mm^2 when targeting the terminals) was performed in ArchT-expressing animals and blue illumination (473 nm) was applied in pulsed mode (10–30 Hz, 10-ms pulse width, ~20 mW/mm^2; ~40 mW/mm^2 when targeting the terminals) in ChR2-expressing animals. Light pulses were generated by a pulse generator (cat. no. 33220A, Meilhaus Electronic GmbH, Germany).

Behavioral tests. All behavioral tests were carried out during the light cycle of the animals.

von Frey test. Mechanical sensitivity was carried out in acclimatized animals via repeated manual applications of von Frey filaments with increasing forces (0.04 to 1 g) to the plantar surface of the hindpaws. In the SNI model, filaments were applied to the lateral region of the hindpaws. Withdrawal frequencies were recorded (5 applications per filament, each applied 30 s apart). Mechanical thresholds were determined by filament forces that elicited ≥40 or ≥60% withdrawal as indicated in the figure legends. The investigator was blinded to the identity of the animals.

Cold plate test. Animals were placed on a 2 °C cold plate and their withdrawal latencies were measured. A cut-off of 30 s was used to prevent potential tissue damage to the paw surfaces.

Capsaicin injection. Capsaicin (Sigma, cat. no. M2028; 0.06%, 20 µl in 10% DMSO/PBS) was injected subcutaneously in the lower hind leg to induce acute secondary mechanical hypersensitivity in the plantar area of the hindpaw. Illumination was carried out for 15 min either at 0, 15 or 30 min after capsaicin injection in opsin-expressing and control animals as indicated in each experimental scheme in figures. Mechanical sensitivity of the hindpaws was measured before and 15 and 45 min after injection in the absence or presence of illumination.

In separate experiments, the durations of observed nocifensive behaviors (licking, paw flicking and paw guarding) in control and ArchT-expressing animals were recorded over a 5-min period after an intraplantar injection of capsaicin, in the presence of yellow illumination in the cortex.

In all the above experiments, capsaicin was injected either in the right paw or right lower hind leg (region above the heel), contralateral to the cortical site of illumination (left hemisphere). The experimenters were blinded to the identity of the mice they were observing and analyzing.

Open field test. The open field test was performed with a 40 × 40 cm box. Each mouse was placed in the center of the box and locomotor activity was recorded for 10 min via a video camera placed above the box. ANY-maze software (Stoelting Co., Ireland) was used to analyze the video recordings. All animals were attached to patch cables and illuminated during the entire 10-min recording. For analysis, the box was divided into grids 3 × 3 square and the middle square was used as the center zone while the surrounding squares were used as the marginal zone. A 3-cm border along the walls of the box was used as the thigmotaxis zone.

Optogenetic conditioned place aversion test. The place aversion test was performed in a custom-made box consisting of two chambers (15 × 15 cm) with distinct visual (vertical versus horizontal stripes) and odor cues. The two chambers were interconnected by a smaller neutral chamber (8 × 8 cm) with detachable doors. A video camera was placed above the setup and ANY-maze software (Stoelting Co., Ireland) was used to record and analyze the videos. All animals were attached to patch cables and placed in the enclosed neutral zone before the doors were removed at the start of each recording.

On day 1, a baseline session was recorded in which all animals were allowed to roam freely between the two testing chambers for 20 min. Animals that spent more than 70% of the recording time in a single testing chamber were excluded

© 2017 Nature America, Inc., part of Springer Nature. All rights reserved.

doi:10.1038/nn.4645

from the experiment. On day 2, animals were placed in their preferred chamber (based on their baseline) for a conditioning session of 30 min (blue light; 20 Hz, 40 ms; 8 s stimulation 2 s pause) as previously described[53]. On day 3 (post-conditioning day), mice were allowed to roam freely between chambers to test their place preferences in the absence of any light trigger.

Slice electrophysiology. Cortical coronal slices through MCC were prepared from mice, age-matched with mice used for behavioral testing. Extraction of the brain and subsequent slicing (300 µm) was done in ice-cold slicing solution (in mM: 85 NaCl, 2.5 KCl, 11.1 glucose, 75 sucrose, 25 $NaHCO_3$, 1.25 NaH_2PO_4, 3 $MgCl_2$, 0.1 $CaCl_2$, 3 3-myo-inositol, 2 sodium pyruvate, 0.4 ascorbic acid, aerated with carbogen (5% CO_2), pH 7.3) on a Leica VT 1200S (Leica Biosystems, Nussloch, Germany). Slices rested at 37 °C for a minimum of 30 min in an incubation solution (in mM: 109 NaCl, 4 KCl, 33.3 glucose, 25 $NaHCO_3$, 1.25 NaH_2PO_4, 1.3 $MgCl_2$, 1.5 $CaCl_2$, 3 3-myo-inositol, 2 sodium pyruvate, 0.4 ascorbic acid, aerated with carbogen, pH 7.3). Electrophysiological recordings were performed on an Olympus BX51WI microscope equipped with a Dodt gradient contrast tube and heating chamber (Badcontroller V, Luigs & Neumann, Germany). The data were amplified, Bessel-filtered at 2.9 and 10 kHz, and digitized at 20 kHz via a HEKA EPC 10 (HEKA Elektronik, Lambrecht, Germany) under the control of PatchMaster. All recordings were performed at near physiological temperatures (35 °C) in artificial cerebrospinal fluid (aCSF) (in mM: 125 NaCl, 2.5 KCl, 16.7 glucose, 25 $NaHCO_3$, 1.25 NaH_2PO_4, 2 $CaCl_2$, 1 $MgCl_2$, aerated with carbogen, pH 7.3). Patch pipettes were pulled from borosilicate glass capillaries and filled with intracellular solution (in mM: 130 potassium gluconate, 20 KCl, 5 disodium phosphocreatine, 10 HEPES, 5 EGTA, 4 Mg-ATP). In some cases 0.1% biocytin was added to the intracellular solution. The blunt-ended light guide was introduced to the recording chamber from the side and positioned above the recorded neurons to yield the maximal light intensity around the neuron recorded from.

The stimulus protocol mimicked the *in vivo* continuous or intermittent protocol for the ArchT-experiments and the 10–30 Hz, 10-ms pulse-width stimulation for ChR2-positive neurons. In the case of the ArchT-mediated inhibition, the light intensity was adjusted to yield roughly 10 mV hyperpolarization. GFP control measurements were done with the maximal intensities (~40 mW/mm^2) used for *in vivo* experiments in the MCC. Adjusting the light intensity ensured that we would get an estimate for *in vivo* neurons independent of expression levels and distance to the light source. For ChR2 experiments, the light intensities used were either as stated or otherwise were maximally at ~20 mW/mm^2. Recordings were performed in current-clamp mode without holding current. As neurons in slices have low spontaneous activity, current injections were given every 2 s with a pulse length of 3 ms and at an amplitude of 20% above threshold, determined at rest. Custom-written scripts scored evoked and spontaneous action potential –like spikes and spikelets. Statistical outliers were defined and removed (defined as 3 times the interquartile range below and above the 25th and 75th percentile, respectively).

***In vivo* single unit recordings.** Four weeks after virus (rAAV-CaMKII-ArchT) injection into the ACC, mice were anesthetized as described above and fixed to a stereotaxic apparatus. A small craniotomy was performed and the dura mater was removed. A microdrive consisting of a Versadrive 4 (Neuralynx, USA) with four independently movable tetrodes and a manually added optic fiber (100 µm in diameter) was chronically implanted. The stripped optic fiber was lowered to the site of MCC injection (0.75 mm depth) and remained in place till the end of the experiment. The tetrodes were made of 12-µm-diameter tungsten wires (H-Formvar insulation with butyral bond coat; California Fine Wire). Two stainless steel screws above the cerebellum served as reference and ground screws. Animals were allowed to recover for 2 weeks before the start of recordings.

During recording, the optic fiber was connected to a 532-nm laser and 10 pulses of 1 s duration were applied to the freely moving animal. In experiments involving capsaicin injection, the mice received 15 min of continuous illumination. Neural signals were acquired using a Digital Lynx 4SX and Cheetah data acquisition software (Neuralynx). For single-unit recordings, signals were bandpass-filtered between 600 Hz and 9,000 Hz and digitized at 32 kHz. Single-unit data were preprocessed with KlustaKwik for automated spike clustering and manually refined using Spikes Sort 3D software (Neuralynx). Further analyses were performed using Neuroexplorer software (Nex Technologies, USA). Responses to capsaicin for individual units were evaluated by comparing the firing rate in spikes per second of 900 s baseline recording to 900 s after injection of capsaicin with a Mann–Whitney rank sum test. Field potentials were bandpass-filtered from 0.1 Hz to 9,000 Hz. Analysis was performed with Brainstorm, which is documented and freely available for download online under the GNU general public license (http://neuroimage.usc.edu/brainstorm/) and custom Matlab scripts (The MathWorks Inc.MA, USA)[54]. A custom-built device was used to trigger mechanical stimulation. The device consisted of a von Frey filament exerting noxious pressure glued on top of a pressure-sensing device connected to an analog channel. One channel per tetrode was used for further analysis. For each trial, responses of all channels were averaged. The area under the curve for each trial was processed for quantification. Each individual trial was normalized to the mean of its own baseline consisting of 20 trials.

Immunocytochemistry. Animals were sacrificed with carbon dioxide overdose and transcardially perfused with phosphate-buffered saline (PBS; pH 7.4) followed by 4% paraformaldehyde (PFA) fixative solution. Brains were removed and postfixed at 4 °C for a further 24 h in PFA. Brain sections (50 µm) were collected with a vibratome, washed in PBS containing 50 mM glycine for 10 min and blocked for 60 min in 10% horse serum and 0.2% Triton in PBS. Sections were incubated in anti-Fos (rabbit; Millipore, catalog number PC38; 1:5,000) in blocking solution overnight at 4 °C. The sections were subsequently washed in 10% horse serum in PBS (two 10 min washes) and incubated with secondary antibody (donkey anti-rabbit Alexa 488 or 594; Jackson Laboratory, catalog numbers 711-545-152 and 711-585-152; 1:700) in washing solution for 1 h at room temperature. Tissues were washed twice in PBS and incubated in DAPI (1:10,000) for 10 min, washed in PBS and incubated for 10 min in 10 mM TRIS-HCl before mounting.

TUNEL labeling and quantification. Postfixed brains were transferred to 30% sucrose and kept at 4 °C for 48 h before cryosections (25 µm) were collected. *In situ* cell death detection was carried out with a TUNEL TMR kit (Roche, Germany) on cortical sections obtained from ArchT-expressing and control animals exposed to *in vivo* illumination (15 min) and perfused (as described above) 60 min after illumination. Positive TUNEL controls were obtained by 10 min incubation with DNase I (3,000 U/mL in 50 mM TRIS-HCl) at room temperature to induce DNA breaks. TUNEL labeling was carried out according to the manufacturer's protocol. An automated quantification of positive TUNEL area was carried out using the ImageJ software (version 1.50e, National Institutes of Health, USA) to auto-detect pixels within an intensity threshold range (determined using negative and positive control samples); the same threshold range was applied to all images. Quantification was measured from the 300 × 300 µm region surrounding the fiber tract and expressed as mean positive area.

Nissl staining and quantification. Postfixed brains were transferred to 30% sucrose for 48 h at 4 °C. Coronal sections (25 µm) were collected with a cryotome and coronal sections within the illuminated region from each animal were sampled randomly and stained for Nissl substance. Sections were imaged on a Leica DM LS2 microscope with either a 20× or a 40× objective. Images were analyzed in a blinded manner. Positive counts were measured from the 300 × 300 µm region surrounding the fiber tract and expressed as mean positive counts.

Fos staining and quantification. Animals were anesthetized with 0.8% isoflurane for 2.5 h to reduce background activity in the brain. Following this, ChR2-expressing animals received a 15 min blue photostimulation while ArchT-expressing animals were injected with capsaicin in the lower hind leg and received a 15-min yellow photostimulation following the injection. Two control groups of ChR2- and ArchT-expressing animals received the same treatment but received no illumination. Animals were perfused 1 h after illumination and coronal sections (50 µm) were sampled across the entire region of interest and processed for Fos as described above. Immunofluorescence was visualized with a laser-scanning confocal microscope (Leica TCS SP2 and SP8, Germany) or Nikon A1 confocal microscope using identical illumination exposure parameters for sections prepared from control and test animals. Sections were sampled at ≥0.05 mm apart across the regions of interest to cover the entire volume and to ensure no double-counting of the same positive cells between sections. All images were subsequently overlaid with the corresponding atlas section[50] to anatomically

© 2017 Nature America, Inc., part of Springer Nature. All rights reserved.

define the regions of interest. ImageJ software (version 1.50a, National Institutes of Health, USA) was used to stereologically count all Fos labeled cells within the boundaries of the defined sites. Positive cells lying on the boundary were excluded. A cell was considered positive only if it displayed an intensity value above the intensity threshold of the background. Experimenters were blinded to the identity of sections they were analyzing. Specificity of the Fos staining was tested on sections from all groups by omitting the primary antibody; in these samples, no immunopositive labeling was found (an example is shown in **Supplementary Fig. 4**).

Statistics. All data are expressed as mean ± s.e.m. in all line graphs and bar graphs overlaid with scatter plots. Box-and-whiskers plots are plotted with 10th, 25th, 75th and 90th percentiles as vertical boxes with error bars; cross lines indicate the medians. *n* numbers represent biological repeats. Two-tailed two-way ANOVA for random measures or two-way ANOVA with repeated measures was used in the analysis of behavioral frequency data; *post hoc* analysis was determined using Bonferroni multiple comparisons. The one-way ANOVA, Mann–Whitney or Kruskal–Wallis ANOVA test followed by *post hoc* Bonferroni test was used to compare data obtained from behavioral thresholds, histological, slice electrophysiological and Fos experiments as indicated in the legends. A normal distribution of the data was tested with the Kolmogorov–Smirnov test if the sample size allowed. No statistical methods were used to predetermine sample sizes, but our sample sizes are similar to those reported in previous publications[8,9,14,28,30]. If the equal-variance assumptions were not valid, statistical significance was evaluated using the Mann–Whitney test. In all tests, a value of $P < 0.05$ was considered significant. SigmaPlot (version 13.0) was used for all statistical analyses. The $F_{(df1, df2)}$, U, H or t statistical test values are reported in the legends; where reported as group $F_{(df1, df2)}$ values, df1 represents degree of freedom for groups and df2 represents degree of freedom for groups × treatments. Where reported as groups × treatment $F_{(df1, df2)}$ values, df1 represents degree of freedom for groups × treatment and df2 represents residual degree of freedom. A detailed **Life Sciences Reporting Summary** is available.

Data availability. The raw data that support the findings of this study are available from the corresponding author upon reasonable request.

46. Dittgen, T. *et al.* Lentivirus-based genetic manipulations of cortical neurons and their optical and electrophysiological monitoring *in vivo*. *Proc. Natl. Acad. Sci. USA* **101**, 18206–18211 (2004).
47. Tang, W. *et al.* Faithful expression of multiple proteins via 2A-peptide self-processing: a versatile and reliable method for manipulating brain circuits. *J. Neurosci.* **29**, 8621–8629 (2009).
48. Smith, R.H., Levy, J.R. & Kotin, R.M. A simplified baculovirus-AAV expression vector system coupled with one-step affinity purification yields high-titer rAAV stocks from insect cells. *Mol. Ther.* **17**, 1888–1896 (2009).
49. During, M.J., Young, D., Baer, K., Lawlor, P. & Klugmann, M. Development and optimization of adeno-associated virus vector transfer into the central nervous system. *Methods Mol. Med.* **76**, 221–236 (2003).
50. Paxinos, G. & Franklin, K.B.J. *The Mouse Brain in Stereotaxic Coordinates* (Academic, 2001).
51. Fillinger, C., Yalcin, I., Barrot, M. & Veinante, P. Afferents to anterior cingulate areas 24a and 24b and midcingulate areas 24a′ and 24b′ in the mouse. *Brain Struct. Funct.* **222**, 1509–1532 (2017).
52. Njoo, C., Heinl, C. & Kuner, R. In vivo siRNA transfection and gene knockdown in spinal cord via rapid noninvasive lumbar intrathecal injections in mice. *J. Vis. Exp.* **85**, 51229 (2014).
53. Barthas, F. *et al.* The anterior cingulate cortex is a critical hub for pain-induced depression. *Biol. Psychiatry* **77**, 236–245 (2015).
54. Tadel, F., Baillet, S., Mosher, J.C., Pantazis, D. & Leahy, R.M. Brainstorm: a user-friendly application for MEG/EEG analysis. *Comput. Intell. Neurosci.* **2011**, 879716 (2011).

© 2017 Nature America, Inc., part of Springer Nature. All rights reserved.

doi:10.1038/nn.4645

nature research

Corresponding author(s): Rohini Kuner

☐ Initial submission ☐ Revised version ☒ Final submission

Life Sciences Reporting Summary

Nature Research wishes to improve the reproducibility of the work that we publish. This form is intended for publication with all accepted life science papers and provides structure for consistency and transparency in reporting. Every life science submission will use this form; some list items might not apply to an individual manuscript, but all fields must be completed for clarity.

For further information on the points included in this form, see Reporting Life Sciences Research. For further information on Nature Research policies, including our data availability policy, see Authors & Referees and the Editorial Policy Checklist.

Experimental design

Sample size

Describe how sample size was determined.

Our sample sizes are also similar to those reported in previous publications (see Methods: Statistics section). In previous studies we have determined the sample size using G-power analyses and therefore have a very clear set of what sample size is required for the behavioral and histochemical data reported.

Data exclusions

Describe any data exclusions.

The sites of injection and viral expression were confirmed at the end of all experiments, animals displaying incorrect expression sites were excluded from all analysis.

Replication

Describe whether the experimental findings were reliably reproduced.

Attempts at replication were successful

Randomization

Describe how samples/organisms/participants were allocated into experimental groups.

Groups were randomized and mice were allocated to experimental groups by a researcher different from the experimentor

Blinding

Describe whether the investigators were blinded to group allocation during data collection and/or analysis.

Experimentor was blinded to the identity of mice being analyzed in behavioral tests

Note: all studies involving animals and/or human research participants must disclose whether blinding and randomization were used.

Statistical parameters

For all figures and tables that use statistical methods, confirm that the following items are present in relevant figure legends (or in the Methods section if additional space is needed).

n/a	Confirmed
☐	☒ The exact sample size (*n*) for each experimental group/condition, given as a discrete number and unit of measurement (animals, litters, cultures, etc.)
☐	☒ A description of how samples were collected, noting whether measurements were taken from distinct samples or whether the same sample was measured repeatedly
☐	☒ A statement indicating how many times each experiment was replicated
☐	☒ The statistical test(s) used and whether they are one- or two-sided (note: only common tests should be described solely by name; more complex techniques should be described in the Methods section)
☐	☒ A description of any assumptions or corrections, such as an adjustment for multiple comparisons
☐	☒ The test results (e.g. *P* values) given as exact values whenever possible and with confidence intervals noted
☐	☒ A clear description of statistics including central tendency (e.g. median, mean) and variation (e.g. standard deviation, interquartile range)
☐	☒ Clearly defined error bars

See the web collection on statistics for biologists for further resources and guidance.

© 2017 Nature America, Inc., part of Springer Nature. All rights reserved.

Nature Neuroscience: doi:10.1038/nn.4645

Software

Policy information about availability of computer code

7. Software

Describe the software used to analyze the data in this study.	Softwares used to analyze the data in this study include Microsoft Excel, SigmaPlot, ANYmaze, Neuroexplorer, ImageJ

For manuscripts utilizing custom algorithms or software that are central to the paper but not yet described in the published literature, software must be made available to editors and reviewers upon request. We strongly encourage code deposition in a community repository (e.g. GitHub). *Nature Methods* guidance for providing algorithms and software for publication provides further information on this topic.

Materials and reagents

Policy information about availability of materials

8. Materials availability

Indicate whether there are restrictions on availability of unique materials or if these materials are only available for distribution by a for-profit company.	No unique materials were used

Antibodies

Describe the antibodies used and how they were validated for use in the system under study (i.e. assay and species).	Antibodies used in this study include rabbit anti-Fos (Millipore; Catalog number PC38), donkey anti-rabbit Alexa Fluor 488 (Jackson Laboratory; Catalog number 711-545-152) or donkey anti-rabbit Alexa Fluor 594 (Jackson Laboratory; Catalog number 711-585-152). Validation of antibody provided in the supplementary (Fig. S4)

9. Eukaryotic cell lines

a. State the source of each eukaryotic cell line used.	no cell lines were used
b. Describe the method of cell line authentication used.	no cell lines were used
c. Report whether the cell lines were tested for mycoplasma contamination.	no cell lines were used
d. If any of the cell lines used are listed in the database of commonly misidentified cell lines maintained by ICLAC, provide a scientific rationale for their use.	no cell lines were used

Animals and human research participants

Policy information about studies involving animals; when reporting animal research, follow the ARRIVE guidelines

11. Description of research animals

Provide details on animals and/or animal-derived materials used in the study.	Adult (8 - 14 weeks) C57Bl6 male wild-type mice (25 - 30 g) were used

Policy information about studies involving human research participants

12. Description of human research participants

Describe the covariate-relevant population characteristics of the human research participants.	No human participants were used

© 2017 Nature America, Inc., part of Springer Nature. All rights reserved.

Nature Neuroscience: doi:10.1038/nn.4645